Advances in Computational Mathematics manuscript No.
(will be inserted by the editor)

Discontinuous Galerkin reduced basis empirical quadrature procedure for model reduction of parametrized nonlinear conservation laws

Masayuki Yano

Received: date / Accepted: date

Abstract We present a model reduction formulation for parametrized nonlinear partial differential equations (PDEs) associated with steady hyperbolic and convection-dominated conservation laws. Our formulation builds on three ingredients: a discontinuous Galerkin (DG) method which provides stability for conservation laws; reduced basis (RB) spaces which provide low-dimensional approximations of the parametric solution manifold; and the empirical quadrature procedure (EQP) which provides hyperreduction of the Galerkin-projection-based reduced model. The hyperreduced system inherits the stability of the DG discretization: (i) energy stability for linear hyperbolic systems, (ii) symmetry and non-negativity for steady linear diffusion systems, and hence (iii) energy stability for linear convection-diffusion systems. In addition, the framework provides (a) a direct quantitative control of the solution error induced by the hyperreduction, (b) efficient and simple hyperreduction posed as a ℓ^1 minimization problem, and (c) systematic identification of the reduced bases and the empirical quadrature rule by a greedy algorithm. We demonstrate the formulation for parametrized aerodynamics problems governed by the compressible Euler and Navier-Stokes equations.

Keywords parametrized nonlinear PDEs · conservation laws · model reduction · hyperreduction · empirical quadrature · discontinuous Galerkin method

1 Introduction

We consider rapid and reliable solution of parametrized nonlinear partial differential equations (PDEs) associated with steady hyperbolic and convection-dominated problems with an emphasis on the compressible Euler and Navier-Stokes equations in aerodynamics. Our interest is in many-query and/or real-time scenarios, which require the solution of the problem for many different parameter values and/or in real time. Our approach to address the problem is model reduction based on offline-online computational decomposition: in the offline stage, which is expensive but performed once, we explore the parameter domain to build a reduced model which captures the essential features of the problem; in the online stage, we invoke many times and/or in real time the reduced model.

Model reduction of nonlinear PDEs requires two ingredients. The first ingredient is a low-dimensional reduce basis (RB) space $\mathcal{V}_N$ of dimension N in which the reduced-model solution (i.e., the RB solution) is sought. In the context of parametrized PDEs, two popular approaches to compute the reduced basis, which spans the reduced space $\mathcal{V}_N$, are the proper orthogonal decomposition (POD), which identifies dominant modes in "snapshots" associated with different parameter values, and the greedy algorithm, which successively computes the bases using a greedy search in the parameter space based on an error estimate. In this work, we employ the latter approach, originally introduced in the reduced basis method, to minimize the number of snapshots computed in the offline stage; we refer to [33,19,31] for reviews of the reduced basis method and the greedy algorithm for parametrized PDEs.

M. Yano
University of Toronto, Institute for Aerospace Studies, 4925 Duffein Street, Toronto, ON, M3H 5T6, Canada
E-mail: myano@utias.utoronto.ca

The second ingredient for model reduction of *nonlinear* PDEs is "hyperreduction", which enables the approximation of the nonlinear residual in $\mathcal{O}(N)$ operations. Specifically, for weak formulations, the evaluation of the residual requires integration over the spatial domain; the goal of hyperreduction is to approximate this integral in $\mathcal{O}(N)$ operations. Hyperreduction approaches for projection-based reduced models fall into two distinct categories. The first class of methods first interpolate the residual using empirical functions and then integrate the interpolated residual. Methods in this class include the gappy POD method [14,10], the empirical interpolation method (EIM) [6,17], the best point interpolation method (BPIM) [24], the missing point estimation (MPE) method [4], and the Gauss-Newton approximate tensor (GNAT) method [11]. The second class of methods are based on a direct evaluation of the residual integrals using empirical, sparse quadrature rules. Methods in this class include the optimal cubature formulation of An et al. [1], the energy-conservative sampling and weighting (ECSW) method of Farhat et al. [15,16], the empirical cubature method of Hernández [18], and our empirical quadrature procedure (EQP) [28,39]. The hyperreduction approach in this work is based on the EQP, which is motivated by the ℓ_1 framework of Ryu and Boyd [34] and provides two attractive features: (i) it provides a direct control of the RB solution error induced by the approximate quadrature; (ii) it efficiently identifies an empirical quadrature rule by solving a ℓ_1 minimization problem cast as a linear program. Specifically, in this work we extend the EQP formulation to discontinuous Galerkin (DG) methods, with an additional emphasis on preserving certain structures of the underlying problem.

The importance of reduced models that preserve the underlying structure of the PDE — especially to ensure the stability of the reduced model applied to complex problems in continuum mechanics — has been highlighted in a number of recent works. For nonlinear problems, both the projection and hyperreduction approaches must be chosen carefully to preserve the structure. In the aforementioned ECSW method [15,16] and in a separate work by Carlberg et al [12], the primary criterion in hyperreduction is to preserve the Lagrangian structure of the problem and to ensure energy stability for nonlinear structural dynamics problems. The energy stability is an important property not only for structural dynamics problems but also for fluid dynamics problems. In the context of model reduction, Barone et al [5] has studied the construction of energy-stable reduced models for the linearized Euler equations. In fact, due to the lack of coercivity, the construction of an energy-stable scheme for hyperbolic and convection-dominated problems is not straightforward even for the full-fidelity (non-reduced) discretizations. The DG method, which is used in this work, is designed specifically to address the stability issue associated with (continuous) Galerkin methods for hyperbolic and convection-dominated problems; for reviews of DG methods, we refer to a general review [13], a review for conservation laws [7], a review for elliptic equations [3], and textbooks [20,32,29]. The DG-EQP hyperreduction procedure proposed in this work preserves this energy stability property of the DG method; hence, in addition to the two aforementioned features, the DG-RB-EQP method provides (iii) energy-stability for linear hyperbolic and convection-dominated systems. We note that the DG method has also been used in the context of model reduction of multiscale elliptic problems [2,27].

Given the application focus of this work on aerodynamic flows, we also note previous work on model reduction for parametrized *and* nonlinear aerodynamic flows. (As the emphasis of this work is on parametrized nonlinear PDEs, we here omit works on *non-parametrized* and/or *linearized* aerodynamic flows.) LeGresley and Alonso [22] considered model reduction of parametrized Euler equations using POD and hyperreduction based on the proximity of the cells to the airfoil. Washabaugh et al considered model reduction of parametrized Euler equations based on local reduced bases (but without hyperreduction) [35] and later extended the work to Reynolds-averaged Navier-Stokes equations using a (global) reduced basis and hyperreduction based on a masking procedure [36]. Zimmermann and Görtz [40] also considered model reduction of parametrized Euler equations using POD but without hyperreduction.

The contribution of this work is fourfold. We first introduce the DG-RB-EQP method, an extension of the EQP to DG methods (Section 3). We second prove various structure-preserving properties of the DG-RB-EQP method; we prove that (a) the method applied to linear hyperbolic systems is energy stable, (b) the method applied to linear diffusion systems preserves the symmetry and non-negativity, and hence (c) the method applied to linear convection-dominated convection-diffusion systems is energy stable (Section 4). We third provide an alternative error estimate for the DG-RB-EQP method that is asymptotically sharper than the original estimate in [39] (Section 4). We finally demonstrate the method for two- and three-dimensional aerodynamic flows governed by the compressible Euler and Navier-Stokes equations (Section 5).

Before we conclude the introduction, we note the scope and limitation of this work. As mentioned in the beginning of the introduction, the two ingredients for model reduction of nonlinear problems are a low-dimensional reduced-basis space and a hyperreduction procedure. As regard the former, one of the known challenges in model reduction of hyperbolic and convection-dominated systems is the approximation of sharp features whose locations are parameter dependent; e.g., moving shear layers in viscous flows and moving shocks in transonic and supersonic flows. In the presence of parameter-dependent discontinuities, the Kolmogorov N-width [30] decays as $\mathcal{O}(N^{-1/2})$ in $L^2(\Omega)$; hence, any model reduction approach based on the approximation of the parametric manifold by a linear space cannot provide a rapidly convergent approximation. For transonic aerodynamics, this limitation of model reduction was recognized from early on [23]. In the past several years, there has been significant effort in the model reduction community to overcome this fundamental limitation through nonlinear approximation; works include [25,21,37] and those in a review paper [26].

While the systematic identification of a low-dimensional approximation space is an important issue, in this work we solely focus on the development of a hyperreduction procedure. As a result, in this work we focus on parametrized subsonic aerodynamic flows, which do not involve shocks; subsonic aerodynamics is important in many applications, including the analysis of unmanned aerial vehicles, gas turbines, and wind turbines. Subsonic Euler flows in particular exhibit neither shocks nor shear layers, and can be rapidly approximated in linear reduced basis spaces, as demonstrated in Section 5. More generally, the formulation presented in this work applies to a broad range of second-order PDEs, including those in heat transfer and elasticity.

2 Discontinuous Galerkin method

2.1 Vector and tensor notations

To concisely describe discretizations for systems of conservation laws, we adhere to the standard vector and tensor notations in this work. Given vectors (i.e., order-1 tensors) $w \in \mathbb{R}^m$ and $v \in \mathbb{R}^m$, their dot product is given by $w \cdot v = \sum_{i=1}^m w_i v_i \in \mathbb{R}$. Given matrices (i.e., order-2 tensors) $W \in \mathbb{R}^{m\times n}$ and $V \in \mathbb{R}^{m\times n}$, their double dot product is given by $W : V = \sum_{i=1}^m \sum_{j=1}^n W_{ij}V_{ij} \in \mathbb{R}$. Given two vectors $w \in \mathbb{R}^m$ and $v \in \mathbb{R}^n$, their outer product is $w \otimes v \in \mathbb{R}^{m\times n}$ whose (i,j) entry is $w_i v_j$. Given an order-4 tensor $K \in \mathbb{R}^{m\times n\times m\times n}$ and an order-2 tensor $V \in \mathbb{R}^{m\times n}$, their product is $KV \in \mathbb{R}^{m\times n}$ whose (i,j) entry is given by $\sum_{k=1}^m \sum_{l=1}^n K_{ijkl}V_{kl}$.

We in addition introduce notations associated with differentiable functions. Given a vector-valued function $v \in H^1(\Omega)^m$ over $\Omega \subset \mathbb{R}^d$, its gradient $\nabla v \in L^2(\Omega)^{m\times d}$ is matrix-valued and is given by $(\nabla v)_{ij} = \frac{\partial v_i}{\partial x_j}$ for $i = 1,\dots,m$ and $j = 1,\dots,d$. Given a matrix-valued function $V \in H^1(\Omega)^{m\times d}$, its divergence $\nabla \cdot V \in L^2(\Omega)^m$ is vector-valued and is given by $(\nabla \cdot V)_i = \sum_{j=1}^d \frac{\partial V_{ij}}{\partial x_j}$ for $i = 1,\dots,m$. Similarly, given a matrix-valued function $V \in H^1(\Omega)^{m\times d}$ and a normal vector n on $\partial\Omega$, their dot product $n \cdot V$ is vector-valued and is given by $(n \cdot V)_i = \sum_{j=1}^d n_j V_{ij}$ for $i = 1,\dots,m$. Note that both the divergence and the dot product with a normal vector contracts the second index of the matrix-valued function.

2.2 Problem statement

We introduce a general form of conservation laws considered in this work. We first introduce a d-dimensional physical domain $\Omega \subset \mathbb{R}^d$ and a P-dimensional parameter domain $\mathcal{D} \subset \mathbb{R}^P$. We then introduce a system of n^c parametrized, steady, nonlinear conservation laws: given $\mu \in \mathcal{D}$, find the state $u(\mu)$ such that

$$\nabla \cdot F(u(\mu);\mu) - \nabla \cdot (K(u(\mu);\mu)\nabla u(\mu)) = 0 \quad \text{in } \Omega, \tag{1}$$

with appropriate boundary conditions; here $F(u(\mu);\mu)$ is the $n^c \times d$-valued parametrized convection flux, $K(u(\mu);\mu)\nabla u(\mu)$ is the $n^c \times d$-valued parametrized viscous flux, $K(u(\mu);\mu)$ is the $n^c \times d \times n^c \times d$-valued parametrized diffusion tensor, and n is the d-valued outward-pointing unit normal on $\partial\Omega$. In general, the convection flux function and the diffusion tensor are nonlinear in both the state and parameter. Many conservation laws can be expressed in this form, including the compressible Euler and Navier-Stokes equations, which are the focus of this work and are considered in Section 5.

2.3 Discontinuous Galerkin method

We now consider discontinuous Galerkin (DG) discretization of the conservation law (1). While we employ the "standard" DG discretization with an upwinded convection flux and the so-called BR2 scheme [8] for the diffusion term, we here briefly review the formulation to facilitate the presentation of our energy-stable element-wise decomposition of the residual in Section 3.1. For more detailed presentations of DG methods, we refer to review papers [3,13,7] and textbooks [20,32,29].

We first introduce a tessellation $\mathcal{T}_h \equiv \{\kappa_i\}_{i=1}^{n^\mathrm{e}}$ of Ω comprising n^e non-overlapping elements so that $\cup_{\kappa\in\mathcal{T}_h}\bar{\kappa} = \bar{\Omega}$ and $\kappa_i \cap \kappa_j = \emptyset$, $i \neq j$; the tessellation comprises polygonal elements with hanging nodes of an arbitrary level. We also introduce a skelton $\Sigma_h \equiv \{\sigma_i\}_{i=1}^{n^\mathrm{f}}$ of $\mathcal{T}_h$ comprising n^f facets; each facet is a facet of at least one element. We identify the boundary and interior facet set by $\Sigma_h^\mathrm{b} \equiv \{\sigma \in \Sigma_h \mid \sigma \cap \partial\Omega \neq \emptyset\}$ and $\Sigma_h^\mathrm{i} \equiv \Sigma_h \setminus \Sigma_h^\mathrm{b}$, respectively; note that each interior facet $\sigma \in \Sigma_h^\mathrm{i}$ has two abutting elements, whereas a boundary facet $\sigma \in \Sigma_h^\mathrm{b}$ has only one abutting element.

We next introduce a discontinuous, piecewise-polynomial approximation space,

$$\mathcal{V}_h \equiv \{v \in (L^2(\Omega))^{n^\mathrm{c}} \mid v|_\kappa \in (\mathbb{P}^p(\kappa))^{n^\mathrm{c}}, \kappa \in \mathcal{T}_h\};$$

the space is endowed with the $L^2(\Omega)$ inner product $(w,v)_{\mathcal{V}_h} \equiv (w,v)_{L^2(\Omega)} \equiv \int_\Omega v \cdot w dx$ and the associated norm $\|w\|_{\mathcal{V}_h} \equiv \sqrt{(w,w)_{\mathcal{V}_h}}$. Note that functions in $\mathcal{V}_h$ are in general discontinuous across element interfaces. Given an interior facet $\sigma \in \Sigma_h^\mathrm{i}$, we identify an element on one side of the facet by $+$ and the other side of the facet by $-$, which are chosen arbitrarily; while the notation is necessary to describe the DG discretization, the final discretization considered in this work is independent of the particular choice. For a boundary facet $\sigma \in \Sigma_h^\mathrm{b}$, without loss of generality, we identify the abutting element by $+$. For $w \in \mathcal{V}_h$, the function evaluated on the $+$ and $-$ side of a facet are denoted by w^+ and w^-, respectively. In addition, given an interior facet $\sigma \in \Sigma_h^\mathrm{i}$, we introduce the following jump and averaging operators [3]. For a function $w \in \mathcal{V}_h$, the averaging operator is given by $\{w\} \equiv \frac{1}{2}(w^+ + w^-)$, the (non-directional) jump operator is given by $[w]_-^+ = w^+ - w^-$, and the directional jump operator is given by $[\![w]\!] \equiv w^+ \otimes n^+ + w^- \otimes n^-$ for $\otimes$ the outer product. We note that the averaging operator $\{\cdot\}$ and the (non-directional) jump operator $[\cdot]_-^+$ are n^c valued; the directional jump operator $[\![\cdot]\!]$ is $n^\mathrm{c} \times d$ valued. In addition, the averaging operator $\{\cdot\}$ and the directional jump operator $[\![\cdot]\!]$ are independent of the order of $+$ and $-$, and hence we do not explicitly denote $+$ and $-$; the (non-directional) jump operator depends on the order of $+$ and $-$, and hence we explicitly denote $+$ and $-$.

We now introduce the DG residual form for the conservation law (1). The DG residual form $r_h : \mathcal{V}_h \times \mathcal{V}_h \times \mathcal{D} \to \mathbb{R}$ is given by

$$r_h(w,v;\mu) = r_h^\mathrm{c}(w,v;\mu) + r_h^\mathrm{d}(w,v;\mu), \tag{2}$$

where $r_h^\mathrm{c} : \mathcal{V}_h \times \mathcal{V}_h \times \mathcal{D} \to \mathbb{R}$ and $r_h^\mathrm{d} : \mathcal{V}_h \times \mathcal{V}_h \times \mathcal{D} \to \mathbb{R}$ are associated with convection and diffusion contributions, respectively. (For notational brevity, here and throughout the work we do not explicitly denote that the statement holds $\forall w, v \in \mathcal{V}_h$ and $\forall \mu \in \mathcal{D}$ when we define a form unless there is an ambiguity.) The convection residual form $r_h^\mathrm{c} : \mathcal{V}_h \times \mathcal{V}_h \times \mathcal{D} \to \mathbb{R}$ is given by

$$r_h^\mathrm{c}(w,v;\mu) \equiv \sum_{\kappa\in\mathcal{T}_h} r_\kappa^{\mathrm{c,e}}(w,v;\mu) + \sum_{\sigma\in\Sigma_h} r_\sigma^{\mathrm{c,f}}(w,v;\mu), \tag{3}$$

where the elemental and facet residual forms are given by

$$r_\kappa^{\mathrm{c,e}}(w,v;\mu) \equiv -\int_\kappa \nabla v : F(w;\mu) dx, \quad \kappa \in \mathcal{T}_h, \tag{4}$$

$$r_\sigma^{\mathrm{c,f}}(w,v;\mu) \equiv \int_\sigma [v]_-^+ \cdot \hat{F}(w^+, w^-; n^+; \mu) ds, \quad \sigma \in \Sigma_h^\mathrm{i}, \tag{5}$$

$$r_\sigma^{\mathrm{c,f}}(w,v;\mu) \equiv \int_\sigma v^+ \cdot \hat{F}^\mathrm{b}(w^+; n^+; \mu) ds, \quad \sigma \in \Sigma_h^\mathrm{b}; \tag{6}$$

here $F(\cdot;\cdot)$ is the aforementioned convection flux function, $\hat{F}(\cdot,\cdot;\cdot;\cdot)$ is the interior numerical flux function, and $\hat{F}^\mathrm{b}(\cdot;\cdot;\cdot)$ is the boundary numerical flux function, which weakly enforces appropriate Dirichlet boundary conditions. We assume that the interior numerical flux is consistent (i.e., $\hat{F}(w,w;n^+;\mu) =$

$n^+ \cdot F(w;\mu)$) and conservative (i.e., $\hat{F}(w^+, w^-; n^+; \mu) = -\hat{F}(w^-, w^+; n^-; \mu)$) and provides appropriate numerical dissipation and hence stability in the DG method; see e.g., [13,7]. The boundary numerical flux function weakly enforces boundary conditions and its precise form depends on the particular condition; here we omit the presentation for brevity.

The diffusion residual form $r_h^{\mathrm{d}} : \mathcal{V}_h \times \mathcal{V}_h \times \mathcal{D} \to \mathbb{R}$ is given by

$$r_h^{\mathrm{d}}(w, v; \mu) = \sum_{\kappa \in \mathcal{T}_h} r_\kappa^{\mathrm{d,e}}(w, v; \mu) + \sum_{\sigma \in \Sigma_h} r_\sigma^{\mathrm{d,f}}(w, v; \mu), \tag{7}$$

where

$$r_\kappa^{\mathrm{d,e}}(w, v; \mu) \equiv \int_\kappa \nabla v : K(w;\mu)\nabla w dx, \quad \kappa \in \mathcal{T}_h, \tag{8}$$

$$r_\sigma^{\mathrm{d,f}}(w, v; \mu) \equiv -\int_\sigma \left(\{K(w;\mu)^T \nabla v\} : [\![w]\!] + [\![v]\!] : \{K(w;\mu)(\nabla w + \theta_\sigma \ell_\sigma([\![w]\!]))\} \right) ds, \quad \sigma \in \Sigma_h^{\mathrm{i}}, \tag{9}$$

$$\begin{aligned} r_\sigma^{\mathrm{d,f}}(w, v; \mu) \equiv -\int_\sigma \Big(& (K(w^+;\mu)^T \nabla v) : ((w^+ - u^{\mathrm{b}}(w^+;\mu)) \otimes n^+) \\ & + (v^+ \otimes n^+) : K(w^+;\mu)(\nabla w^+ + \theta_\sigma \ell_\sigma^{\mathrm{b}}(w^+;\mu)) \Big) ds, \quad \sigma \in \Sigma_h^{\mathrm{b}}. \end{aligned} \tag{10}$$

Here, $u^{\mathrm{b}}(\cdot;\cdot)$ provides the Dirichlet boundary value. The interior lifting operator $\ell_\sigma(\cdot)$ provides, for a vector jump $[\![w]\!]$ on $\sigma \in \Sigma_h^{\mathrm{i}}$, the matrix-valued lifted function $\ell_\sigma([\![w]\!]) \in (\mathcal{V}_h)^d$ that has the support over the two abutting elements κ^+ and κ^- and satisfies

$$\int_{\kappa^+ \cup \kappa^-} v : \ell_\sigma([\![w]\!]) dx = -\int_\sigma \{v\} : [\![w]\!] ds, \quad \forall v \in (\mathcal{V}_h)^d. \tag{11}$$

Similarly, the boundary lifting operator $\ell_\sigma^{\mathrm{b}}(\cdot)$ provides, for a trace w^+ on $\sigma \in \Sigma_h^{\mathrm{b}}$, the lifted function $\ell_\sigma^{\mathrm{b}}(w^+) \in (\mathcal{V}_h)^d$ that has the support over the abutting element κ^+ and satisfies

$$\int_{\kappa^+} v : \ell_\sigma^{\mathrm{b}}(w^+;\mu) dx = -\int_\sigma v : ((w^+ - u^{\mathrm{b}}(w^+;\mu)) \otimes n^+) ds, \quad \forall v \in (\mathcal{V}_h)^d. \tag{12}$$

The BR2 penalty parameter $\theta_\sigma \in \mathbb{R}_{>0}$ on each facet is chosen to be greater than the maximum number of facets on the abutting elements. In the presence of hanging nodes, the total number of divided facets is counted; e.g., if a quadrilateral element has a hanging node on two of its facets, then the total number of facets is six. In practice we set θ_σ equal to twice the maximum total number of facets on the abutting elements. While these particular lifting operators are used in the BR2 formulation, there also exist other choices of lifting operators (see, e.g., [3]).

Having defined the residual form (2), the DG-FEM "truth" approximation is given by the following: given $\mu \in \mathcal{D}$, find $u_h(\mu) \in \mathcal{V}_h$ such that

$$r_h(u_h(\mu), v_h; \mu) = 0 \quad \forall v_h \in \mathcal{V}_h. \tag{13}$$

We assume that the "truth" problem is well posed and refer to $u_h(\mu) \in \mathcal{V}_h$ as the "truth" solution.

2.4 Nonlinear solver: pseudo-time continuation

As (13) is nonlinear in $u_h(\mu)$, we employ a pseudo-time continuation (PTC) procedure to reliably solve the nonlinear algebraic system. An effective PTC strategy depends on the specific conservation law; we here describe our strategy for the compressible Euler and Navier-Stokes equations. We first introduce the time-dependent counterpart of (13): given $\mu \in \mathcal{D}$, find $u_h^{\mathrm{ptc}}(t;\mu) \in \mathcal{V}_h$ such that

$$\begin{aligned} \int_\Omega v_h \frac{\partial u_h^{\mathrm{ptc}}(t;\mu)}{\partial t} dx + r_h(u_h^{\mathrm{ptc}}(t;\mu), v_h; \mu) = 0 \quad \forall v_h \in \mathcal{V}_h, \ \forall t \in \mathbb{R}_{>0}, \\ u_h^{\mathrm{ptc}}(t=0;\mu) = u_h^0(\mu), \end{aligned}$$

where $u_h^0(\mu)$ is a suitable initial state, which for aerodynamic flows is often the freestream condition. We then apply the backward Euler method to the unsteady equation and march forward in (pseudo)

time until the steady state solution is obtained. As our interest is only in the steady-state solution, we adaptively increase the time-step size in the solution process; in each step, we also monitor the changes in the density and pressure at all quadrature points and, as necessary, backtrack such that the changes in the quantities are smaller than a prescribed threshold value. We refer to [38] for a detailed presentation of the particular PTC strategy employed in this work.

3 Discontinuous Galerkin reduced basis empirical quadrature procedure

The empirical quadrature procedure (EQP) approximates the finite element residual using a small subset of quadrature points. In our original EQP formulation for continuous Galerkin finite element methods [39], we decompose the finite element residual to the level of quadrature points. In the current work on an EQP formulation for DG methods, we decompose the DG residual instead to the level of elements and not quadrature points. This element-wise decomposition, instead of quadrature-point-wise decomposition, is motivated by two factors. First, as mentioned in the Introduction, one of our goals is to ensure that the EQP hyperreduced model remains energy stable for linear hyperbolic and convection-dominated problems; using a carefully chosen element-wise decomposition is one way to achieve this goal. Second, the element-wise decomposition allows us to leverage the fast and vectorized element-wise residual evaluation routines implemented in many DG code.

We achieve the construction of energy-stable and accurate hyperreduced model in two steps. We first devise an element-wise decomposition of the DG residual form (2) such that each elemental residual form is energy stable (Section 3.1); the choice implies that the hyperreduced model based on *any* subset of elements will be energy stable. We second invoke the EQP procedure to identify a subset of elements which yields a hyperreduced model (i) that meets the accuracy requirement and (ii) such that only a small number of elements are involved in residual evaluations (Section 3.3).

3.1 Energy-stable element-wise decomposition of the DG residual

In this section we identify an element-wise decomposition of the DG residual form (2)

$$r_h(w, v; \mu) \equiv \sum_{\kappa \in \mathcal{T}_h} \eta_\kappa(w, v; \mu) \tag{14}$$

for

$$\eta_\kappa(w, v; \mu) \equiv \eta_\kappa^{\mathrm{c}}(w, v; \mu) + \eta_\kappa^{\mathrm{d}}(w, v; \mu) \tag{15}$$

such that each elemental convection residual form $\eta_\kappa^{\mathrm{c}}(\cdot, \cdot; \mu)$ is energy stable for linear hyperbolic systems (in the sense made more precise in Section 4.1) and each elemental diffusion residual form $\eta_\kappa^{\mathrm{d}}(\cdot, \cdot; \mu)$ is symmetric and non-negative for linear diffusion systems (in the sense made more precise in Section 4.2). We note that we use the term "element-wise" to indicate that the residual is expressed as a sum of the terms associated with elements in the sense of (14). However, the evaluation of the individual $\eta_\kappa(w, v; \mu)$ in general requires the values of the functions w and v on not just the element κ but also its neighbor elements as the DG residual on a facet depends on the state of all abutting elements. Hence, "element-wise" does not imply the evaluation of $\eta_\kappa(w, v; \mu)$ only depends on the function values over κ.

We define an energy-stable elemental convection residual form $\eta_\kappa^{\mathrm{c}} : \mathcal{V}_h \times \mathcal{V}_h \times \mathcal{D} \to \mathbb{R}$ as follows:

$$\eta_\kappa^{\mathrm{c}}(w, v; \mu) \equiv r_\kappa^{\mathrm{c,e}}(w, v; \mu) + \sum_{\sigma \in \partial\kappa \cap \Sigma_h^{\mathrm{i}}} r_{\sigma,\kappa}^{\mathrm{c,f,split}}(w, v; \mu) + \sum_{\sigma \in \partial\kappa \cap \Sigma_h^{\mathrm{b}}} r_\sigma^{\mathrm{c,f}}(w, v; \mu), \tag{16}$$

where $r_\kappa^{\mathrm{c,e}}(\cdot, \cdot; \cdot)$ for $\kappa \in \mathcal{T}_h$ and $r_\sigma^{\mathrm{c,f}}(\cdot, \cdot; \cdot)$ for $\sigma \in \Sigma_h^{\mathrm{b}}$ are as defined in (4) and (6), respectively, and $r_{\sigma,\kappa}^{\mathrm{c,f,split}}(\cdot, \cdot; \cdot)$ for the elements on the $+$ and $-$ side of $\sigma \in \Sigma_h^{\mathrm{i}}$ is given by

$$r_{\sigma,\kappa^\pm}^{\mathrm{c,f,split}}(w, v; \mu) \equiv \int_\sigma \left(\frac{1}{4}[(v \otimes n) : F(w; \mu)]_\mp^\pm + \frac{1}{2}[v]_-^+ \cdot \hat{F}(w^+, w^-; n^+; \mu) \right) ds. \tag{17}$$

More explicitly, the first term evaluates to $(v^+ \otimes n^+) : F(w^+; \mu) - (v^- \otimes n^-) : F(w^-; \mu)$ for the element κ^+ on the $+$ side, and the term evaluates to $(v^- \otimes n^-) : F(w^-; \mu) - (v^+ \otimes n^+) : F(w^+; \mu)$ for the element

κ^- on the $-$ side; the second term is independent of the side to which the element belongs because $[v]^+_- \cdot \hat{F}(w^+, w^-; n^+; \mu) = [v]^-_+ \cdot \hat{F}(w^-, w^+; n^-; \mu)$ by the conservative property of the numerical flux. We note that this element-wise split interior facet residual is consistent with the original facet residual $r^{\mathrm{c,f}}_\sigma(w, v; \mu)$ for $\sigma \in \Sigma^{\mathrm{i}}_h$ defined in (5) in the sense that the sum of the residuals for the $+$ and $-$ elements yields

$$r^{\mathrm{c,f,split}}_{\sigma,\kappa^+}(w, v; \mu) + r^{\mathrm{c,f,split}}_{\sigma,\kappa^-}(w, v; \mu) = \int_\sigma [v]^+_- \cdot \hat{F}(w^+, w^-; n^+; \mu) ds = r^{\mathrm{c,f}}_\sigma(w, v; \mu).$$

It follows that $\sum_{\kappa\in\mathcal{T}_h} \eta^{\mathrm{c}}_\kappa(w, v; \mu) = r^{\mathrm{c}}_h(w, v; \mu)$, and hence $\eta^{\mathrm{c}}_\kappa(\cdot, \cdot; \cdot)$ merely provides an alternative decomposition of the convection residual form (3); however as we will see in Section 4.1, the elemental residual (16) is energy stable for linear hyperbolic systems.

We next define an energy-stable elemental diffusion residual form $\eta^{\mathrm{c}}_\kappa : \mathcal{V}_h \times \mathcal{V}_h \times \mathcal{D} \to \mathbb{R}$ as follows:

$$\eta^{\mathrm{d}}_\kappa(w, v; \mu) \equiv r^{\mathrm{d,e}}_\kappa(w, v; \mu) + \sum_{\sigma\in\partial\kappa\cap\Sigma^{\mathrm{i}}_h} r^{\mathrm{d,f,split}}_{\sigma,\kappa}(w, v; \mu) + \sum_{\sigma\in\partial\kappa\cap\Sigma^{\mathrm{b}}_h} r^{\mathrm{d,f}}_\sigma(w, v; \mu) \tag{18}$$

where $r^{\mathrm{d,e}}_\kappa(\cdot, \cdot; \cdot)$ for $\kappa \in \mathcal{T}_h$ and $r^{\mathrm{d,f}}_\sigma(\cdot, \cdot; \cdot)$ for $\sigma \in \Sigma^{\mathrm{b}}_h$ are as defined in (8) and (10), respectively, and $r^{\mathrm{d,f,split}}_{\sigma,\kappa}(\cdot, \cdot; \cdot)$ for the element on the $+$ and $-$ side of $\sigma \in \Sigma^{\mathrm{i}}_h$ is given by

$$r^{\mathrm{d,f,split}}_{\sigma,\kappa^\pm}(w, v; \mu) \equiv -\int_\sigma \left(\frac{1}{2}\nabla v^\pm : K(w^\pm; \mu)[\![w]\!] + \frac{1}{2}[\![v]\!] : K(w^\pm; \mu)(\nabla w^\pm + \theta_\sigma \ell^\pm_\sigma([\![w]\!])) \right) ds. \tag{19}$$

Similarly to the convection residual, we note that this element-wise split interior facet residual is consistent with the original facet residual $r^{\mathrm{d,f}}_\sigma(\cdot, \cdot; \cdot)$ for $\sigma \in \Sigma^{\mathrm{i}}_h$ defined in (9) in the sense that the sum of the residuals for the $+$ and $-$ elements yields

$$\begin{aligned} &r^{\mathrm{d,f,split}}_{\sigma,\kappa^+}(w, v; \mu) + r^{\mathrm{d,f,split}}_{\sigma,\kappa^-}(w, v; \mu) \\ &\quad = -\int_\sigma \left(\{K(w; \mu)^T \nabla v\} : [\![w]\!] + [\![v]\!] : \{K(w; \mu)(\nabla w + \theta_\sigma \ell_\sigma([\![w]\!]))\} \right) ds = r^{\mathrm{d,f}}_\sigma(w, v; \mu). \end{aligned}$$

It again follows that $\sum_{\kappa\in\mathcal{T}_h} \eta^{\mathrm{d}}_\kappa(w, v; \mu) = r^{\mathrm{d}}_h(w, v; \mu)$, and hence $\eta^{\mathrm{d}}_\kappa(\cdot, \cdot; \cdot)$ merely provides an alternative decomposition of the diffusion residual form (7); however, as we will in Section 4.2, the elemental residual (18) is symmetric and non-negative for linear diffusion systems.

3.2 Reduced-basis approximation

We now consider a reduced basis approximation of the DG-FEM problem (13). To this end, we introduce a reduced basis space $\mathcal{V}_N \equiv \mathrm{span}\{u_h(\mu)\}_{\mu\in\Xi^{\mathrm{rb}}_N} \subset \mathcal{V}_h$ associated with a snapshot parameter set $\Xi^{\mathrm{rb}}_N \subset \mathcal{D}$ of size N. The snapshot parameter set and the associated reduced basis are hierarchical in the sense that $\Xi^{\mathrm{rb}}_{N=1} \subset \cdots \subset \Xi^{\mathrm{rb}}_{N=N_{\max}}$ and $\mathcal{V}_{N=1} \subset \cdots \subset \mathcal{V}_{N=N_{\max}}$. The snapshot parameter sets are constructed using the greedy algorithm discussed in Section 3.4. The associated "truth"-quadrature reduced basis problem is as follows: given $\mu \in \mathcal{D}$, find $u_N(\mu) \in \mathcal{V}_N$ such that

$$r_h(u_N(\mu), v_N; \mu) = 0 \quad \forall v_N \in \mathcal{V}_N. \tag{20}$$

We assume that the problem is well posed and refer to $u_N(\mu) \in \mathcal{V}_N$ as the "truth"-quadrature RB solution or, more simply, the RB solution. In practice, we solve the nonlinear problem (20) using the pseudo-time continuation strategy discussed in Section 2.4.

We now introduce a discrete form of the RB problem (20) to facilitate the discussion of our hyperreduction procedure in Section 3.3. By way of preliminaries, we introduce $\mathcal{V}_h$-orthonormal basis $\{\phi_i\}_{i=1}^{N_{\max}}$ such that $\mathcal{V}_N = \mathrm{span}\{\phi_i\}_{i=1}^N$, $N = 1, \ldots, N_{\max}$. We also introduce the associated reduced basis operator $Z_N : \mathbb{R}^N \to \mathcal{V}_N$ which maps a generalized coordinate $\mathbf{w} \in \mathbb{R}^N$ to the associated field $w = Z_N\mathbf{w} \equiv \sum_{i=1}^N \mathbf{w}_i\phi_i \in \mathcal{V}_N$. We then introduce the discrete residual form $\mathbf{r}_N : \mathbb{R}^N \times \mathcal{D} \to \mathbb{R}^N$ such that

$$\mathbf{r}_N(\mathbf{w}; \mu) \equiv \sum_{\kappa\in\mathcal{T}_h} \boldsymbol{\eta}_{N,\kappa}(\mathbf{w}; \mu), \tag{21}$$

where the discrete reduced basis element residual form $\boldsymbol{\eta}_{N,\kappa} : \mathbb{R}^N \times \mathcal{D} \to \mathbb{R}^N$ satisfies

$$\boldsymbol{\eta}_{N,\kappa}(\mathbf{w};\mu)_i \equiv \eta_\kappa(Z_N\mathbf{w}, \phi_i; \mu), \quad \forall i = 1, \ldots, N.$$

We also introduce the associated Jacobian $\mathbf{J}_N : \mathbb{R}^N \times \mathcal{D} \to \mathbb{R}^{N\times N}$ such that

$$\mathbf{J}_N(\mathbf{w};\mu)_{ij} \equiv \left.\frac{\partial \mathbf{r}_N(\mathbf{v};\mu)_i}{\partial \mathbf{v}_j}\right|_{(\mathbf{w},\mu)} = r'_h(Z_N\mathbf{w}; \phi_j, \phi_i; \mu), \quad \forall i, j = 1, \ldots, N, \tag{22}$$

where $r'_h(Z_N\mathbf{w}; \phi_j, \phi_i; \mu)$ is the Gâteaux derivative of $r_h(\cdot, \phi_i; \mu)$ at $Z_N\mathbf{w}$ in the direction ϕ_j; for convenience, we refer to $r'_h(\cdot;\cdot,\cdot;\cdot)$ as a Jacobian form. The discrete form of the RB problem (20) is as follows: given $\mu \in \mathcal{D}$, find $\mathbf{u}_N(\mu) \in \mathbb{R}^N$ such that

$$\mathbf{r}_N(\mathbf{u}_N(\mu);\mu) = 0 \quad \text{in } \mathbb{R}^N; \tag{23}$$

the RB solution is given by $u_N(\mu) = Z_N\mathbf{u}_N(\mu)$.

3.3 Empirical quadrature procedure (EQP)

We now consider an EQP approximation of the RB problem (20) and in particular the (discrete) RB problem (23). Our procedure is a modification of the RB-EQP procedure for (continuous) Galerkin methods [39] to discontinuous Galerkin methods with an emphasis on preserving energy stability. As discussed in the introduction to Section 3, we achieve energy stability in two steps: we first identify an element-wise energy-stable splitting of the DG residual; we then select a subset of elements to estimate the residual. The first step was discussed in Section 3.1; we now discuss the application of the EQP for the second step.

We introduce the RB-EQP residual form $r^\nu : \mathcal{V}_h \times \mathcal{V}_h \times \mathcal{D} \to \mathbb{R}^N$ such that

$$r^\nu(w, v; \mu) \equiv \sum_{\kappa\in\mathcal{T}_h} \rho^\nu_\kappa \eta_\kappa(w, v; \mu), \tag{24}$$

where $\eta_\kappa(\cdot,\cdot;\cdot)$ is the energy-stable elemental residual form (15) and $\{\rho^\nu_\kappa\}_{\kappa\in\mathcal{T}_h}$ are the EQP weights determined by a linear programming procedure introduced shortly. The RB-EQP problem is as follows: find $u^\nu_N(\mu) \in \mathbb{R}^N$ such that

$$r^\nu(u^\nu_N(\mu), v; \mu) = 0 \quad \forall v \in \mathcal{V}_N. \tag{25}$$

To facilitate the presentation of the RB-EQP procedure, we also introduce the discrete residual form $\mathbf{r}^\nu_N : \mathbb{R}^N \times \mathcal{D} \to \mathbb{R}^N$ given by

$$\mathbf{r}^\nu_N(\mathbf{w};\mu) \equiv \{r^\nu(Z_N\mathbf{w}, \phi_i; \mu)\}_{i=1}^N = \sum_{\kappa\in\mathcal{T}_h} \rho^\nu_\kappa \boldsymbol{\eta}_{N,\kappa}(\mathbf{w};\mu), \tag{26}$$

and the associated (discrete) RB-EQP solution, $\mathbf{u}^\nu_N(\mu) \in \mathbb{R}^N$ such that

$$\mathbf{r}^\nu_N(\mathbf{u}^\nu_N(\mu);\mu) = 0 \quad \text{in } \mathbb{R}^N; \tag{27}$$

note that $u^\nu_N(\mu) = Z_N\mathbf{u}^\nu_N(\mu)$. In practice, we compute the solution to (25) (or equivalently (27)) using the pseudo-time continuation strategy discussed in Section 2.4.

We now wish to identify EQP quadrature weights $\{\rho^\nu_\kappa\}_{\kappa\in\mathcal{T}_h}$ for the hyperreduced residual (24) (or equivalently the discrete counterpart (26)) such that (i) the weights are sparse (i.e., mostly zero) to facilitate fast evaluations of the residual but (ii) the associated solution $u^\nu_N(\mu)$ is accurate in the sense that $\|u_N(\mu) - u^\nu_N(\mu)\|_{\mathcal{V}_h}$ is small for all $\mu \in \mathcal{D}$. Our algorithm to identify the EQP quadrature weights is informed by the error analysis provided in Section 4.4; we here merely present the algorithm and defer the discussions of the design of the algorithm to Section 4.4. To introduce the algorithm, following [39], we specify (a) an accuracy parameter $\delta \in \mathbb{R}_{>0}$, (b) a parameter training set $\Xi^{\text{train}}_J \equiv \{\mu^{\text{train}}_j\}_{j=1}^J \subset \mathcal{D}$ of size J, and (c) the associated state training set $\{u^{\text{train}}_N(\mu)\}_{\mu\in\Xi^{\text{train}}_J} = \{Z_N\mathbf{u}^{\text{train}}_N(\mu)\}_{\mu\in\Xi^{\text{train}}_J} \subset \mathcal{V}_N$. We then consider a linear programming (LP) problem $\texttt{LP}^\nu_N$: find a basic feasible solution $\{\rho\}_{\kappa\in\mathcal{T}_h}$ such that

$$\rho^{\nu,\star} = \arg\min_{\rho\in\mathbb{R}^{n_e}} \sum_{\kappa\in\mathcal{T}_h} \rho^\nu_\kappa$$

subject to n^{e} non-negativity constraints

$$\rho_\kappa^\nu \geq 0 \quad \forall \kappa \in \mathcal{T}_h,$$

the constant-function accuracy constraint

$$\left| |\Omega| - \sum_{\kappa \in \mathcal{T}_h} \rho_\kappa^\nu |\kappa| \right| \leq \delta |\Omega|,$$

and NJ manifold accuracy constraints

$$\left\| \mathbf{J}_N(\mathbf{u}_N^{\mathrm{train}}(\mu);\mu)^{-1} \left(\mathbf{r}_N(\mathbf{u}_N^{\mathrm{train}}(\mu);\mu) - \sum_{\kappa \in \mathcal{T}_h} \rho_\kappa^\nu \boldsymbol{\eta}_{N,\kappa}(\mathbf{u}_N^{\mathrm{train}}(\mu);\mu) \right) \right\|_\infty \leq \frac{\delta}{\sqrt{N}} \quad \forall \mu \in \Xi_J^{\mathrm{train}}. \tag{28}$$

The solution to $\mathtt{LP}_N^\nu$ provides the EQP weights for (24) (or equivalently (26)). We provide error estimates for the hyperreduction error $\|u_N(\mu) - u_N^\nu(\mu)\|_{\mathcal{V}_h}$ in Section 4.4.

3.4 Greedy algorithm: simultaneous training of RB and EQP

We now discuss a systematic procedure to find the reduced basis $\{\phi_i\}_{i=1}^N$ and the associated EQP weights $\{\rho_\kappa\}_{\kappa \in \mathcal{T}_h}$. To this end, we employ the greedy algorithm devised in [39], which is reproduced as Algorithm 1 for completeness. We here provide a brief description and refer to [39] for a complete description. The algorithm takes as input a training set $\Xi_J^{\mathrm{train}} \subset \mathcal{D}$, the EQP tolerance $\delta \in \mathbb{R}_{>0}$, and the RB residual tolerance $\delta^{\mathrm{rb}} \in \mathbb{R}_{>0}$. It then outputs the reduced basis $\{\phi_i\}_{i=1}^N$ and the associated EQP weights $\{\rho_\kappa^\nu\}_{\kappa \in \mathcal{T}_h}$. In each greedy iteration, the algorithm evaluates the RB-EQP solution $u_N^\nu(\mu)$ and the associated dual norm of the "truth" residual $\|r_h(u_N^\nu(\mu), \cdot; \mu)\|_{\mathcal{V}_h'} \equiv \sup_{v \in \mathcal{V}_h} |r_h(u_N^\nu(\mu), v; \mu)|/|v|_{\mathcal{V}_h}$ for all $\mu \in \Xi_J^{\mathrm{train}}$ and then chooses the parameter that is least-well represented (i.e., maximizes the "truth" residual) as $\mu^{(N)}$ (line 6). It then computes the "truth" solution $u_h(\mu^{(N)})$ by solving the "truth" DG problem (13) (line 9). The algorithm then updates the snapshot parameter set Ξ_N^{rb} and the associated reduced basis $\{\phi_i\}_{i=1}^N$ (line 10). It finally solves the EQP linear program $\mathtt{LP}_N^\nu$ to find the associated EQP weights $\{\rho_\kappa^\nu\}_{\kappa \in \mathcal{T}_h}$ (lines 11-20). We here "bootstrap" and use for the "best-available" state as the training state $\{u_N^{\mathrm{train}}(\mu)\}_{\mu \in \Xi_J^{\mathrm{train}}}$ in smoothing iterations $i = 1, \ldots, N_{\mathrm{eqp,smooth}}$. Specifically, we proceed as follows: (i) in the very first iteration ($i = 1$ and $N = 1$), we set the training state $u_N^{\mathrm{train}}(\mu)$ to $u_h(\mu^{(N=1)})$ for all parameter values, which is a crude but the only available approximation; (ii) for $i = 1$ but $N \neq 1$, we set the training state $u_N^{\mathrm{train}}(\mu)$ to the "truth" solution $u_h(\mu)$ for $\mu \in \Xi_N^{\mathrm{rb}}$ and to the DG-RB-EQP approximation $u_{N-1}^\nu(\mu)$ (and not $u_N^\nu(\mu)$) for $\mu \in \Xi_J^{\mathrm{train}} \setminus \Xi_N^{\mathrm{rb}}$ since the EQP rule has not been updated for the new RB of size N; (iii) for $i > 1$, we set the training state to the "truth" solution $u_h(\mu)$ for $\mu \in \Xi_N^{\mathrm{rb}}$ and to the DG-RB-EQP approximation $u_N^\nu(\mu)$ for $\mu \in \Xi_J^{\mathrm{train}} \setminus \Xi_N^{\mathrm{rb}}$. The number of smoothing iterations of $N_{\mathrm{eqp,smooth}} = 3$ is used in this work. As discussed shortly and shown in numerical examples in Section 5, one of the dominant costs of the offline training is associated with the construction of the EQP linear program; we hence wish to minimize the number of smoothing iterations. For the aerodynamics problems considered in this work and for the hyperelasticity problem considered in [39], we have found $N_{\mathrm{eqp,smooth}} = 3$ is sufficient for the number of EQP elements to "converge" in the "bootstrap" strategy; the ability of the strategy to yield the quadrature rule that meets the desired error tolerance will be demonstrated numerically in Section 5.

We briefly remark on the computational cost. Each greedy iteration requires (i) one evaluation of the "truth" solution (line 9), (ii) $J \cdot (N_{\mathrm{eqp,smooth}} + 1) = |\Xi_J^{\mathrm{train}}| \cdot (N_{\mathrm{eqp,smooth}} + 1)$ evaluations of the "truth" residual (lines 6 and 13), and (iii) $J \cdot N_{\mathrm{eqp,smooth}}$ evaluation of the DG-RB-EQP solutions (lines 6 and 13). The dominant cost for the algorithm are (i) and (ii), which requires the evaluation of "truth" quantities. For nonlinear problems, the cost associated with the *solution* evaluation is significantly higher than the *residual* evaluation, as the former requires multiple PTC (or Newton) iterations, each of which requires a residual evaluation, a Jacobian evaluation, and a linear solve. Hence, the cost for the single solution in (i) can be comparable to the cost for multiple residuals in (ii). Consequently, the overall computational cost to construct a (hyper)reduced model of dimension N is comparable to the cost for N "truth" solution evaluations. We will confirm this behavior in Section 5.

Algorithm 1: Greedy algorithm for simultaneous RB and EQP training.

inputs : parameter training set: $\Xi_J^{\text{train}} \subset \mathcal{D}$
EQP tolerance: $\delta \in \mathbb{R}_{\geq 0}$
RB residual tolerance: $\delta^{\text{rb}} \in \mathbb{R}_{>0}$
outputs: reduced basis: $\{\phi_i\}_{i=1}^{N_{\max}}$
EQP weights: $\{\rho_\kappa^\nu\}_{\kappa \in \mathcal{T}_h}$

Set $\Xi_{N=0}^{\text{rb}} = \emptyset$, $\{\phi_i\}_{i=1}^{0} = \emptyset$.
for $N = 1, \ldots, N_{\max}$ **do**
  if $N = 1$ **then**
    Set $\mu^{(N)} = \arg\inf_{\mu \in \Xi_J^{\text{train}}} \|\bar{\mu} - \mu\|$ where $\bar{\mu} \equiv \frac{1}{N} \sum_{\mu \in \Xi_J^{\text{train}}} \mu$.
  else
    Set $\mu^{(N)} = \arg\sup_{\mu \in \Xi_J^{\text{train}}} \|r_h(u_{N-1}^\nu(\mu), \cdot; \mu)\|_{(\mathcal{V}_h)'}$.
  end
  If $\|r_h(u_{N-1}(\mu^{(N)}); \mu)\|_{(\mathcal{V}_h)'} < \delta^{\text{rb}}$, terminate.
  Find "truth" solution $u_h(\mu^{(N)}) \in \mathcal{V}_h$.
  Update reduced basis: $\Xi_N^{\text{rb}} = \Xi_{N-1}^{\text{rb}} \cup \mu^{(N)}$, $\{\phi_i\}_{i=1}^{N} = \text{Gram-Schmidt}_{\mathcal{V}}\{\phi_1, \ldots, \phi_{N-1}, u_h(\mu^{(N)})\}$.
  for $i = 1, \ldots, N_{\text{eqp,smooth}}$ **do**
    if $i = 1$ ***and*** $N = 1$ **then**
      Set $u_N^{\text{train}}(\mu) = u_h(\mu^{(N=1)}), \quad \mu \in \Xi_J^{\text{train}}$
    else if $i = 1$ **then**
      Set $u_N^{\text{train}}(\mu) = \begin{cases} u_h(\mu), & \mu \in \Xi_N^{\text{rb}} \\ u_{N-1}^\nu(\mu), & \mu \in \Xi_J^{\text{train}} \setminus \Xi_N^{\text{rb}} \end{cases}$
    else
      Set $u_N^{\text{train}}(\mu) = \begin{cases} u_h(\mu), & \mu \in \Xi_N^{\text{rb}} \\ u_N^\nu(\mu), & \mu \in \Xi_J^{\text{train}} \setminus \Xi_N^{\text{rb}} \end{cases}$
    end
    Solve $\texttt{LP}_N^\nu$ for $\nu \equiv \{\delta, \Xi_J^{\text{train}}, \{u_N^{\text{train}}(\mu)\}_{\mu \in \Xi_J^{\text{train}}}\}$ to update $\{\rho_\kappa^\nu\}_{\kappa \in \mathcal{T}_h}$.
  end
end

4 Analysis

We now analyze various properties of the DG-RB-EQP discretization devised in Section 3. In Section 4.1 we analyze the energy stability for linear hyperbolic systems. In Section 4.2 we analyze the symmetry and non-negativity for linear diffusion systems. In Section 4.3 we analyze the energy stability for convection-diffusion systems. In Section 4.4 we provide *a priori* error estimates for the formulation. For notational brevity, we will not explicitly denote the parametric dependence of various forms and functions throughout this section.

4.1 Energy stability for linear hyperbolic systems

We first consider the application of the DG-RB-EQP formulation to a linear hyperbolic system

$$\begin{aligned} \frac{\partial u}{\partial t} + \nabla \cdot (Au) = 0 \quad &\text{in } \Omega \times (0, T], \\ A(n)^- u = A(n)^- u^{\text{b}} \quad &\text{on } \partial\Omega \times (0, T], \\ u(t = 0) = u^0 \quad &\text{in } \Omega \times \{0\}, \end{aligned} \tag{29}$$

where Au is the $n^{\text{c}} \times d$-valued flux function, $A \in \mathbb{R}^{n^{\text{c}} \times d \times n^{\text{c}}}$ is the flux tensor that is symmetric in the sense that $A_{ikj} = A_{jki}$ for $i, j = 1, \ldots, n^{\text{c}}$, $A(n) \in \mathbb{R}^{n^{\text{c}} \times n^{\text{c}}}$ the directional flux tensor given by $A(n)_{ij} = \sum_{k=1}^{d} n_k A_{ikj}$, $A(n)^- \equiv \frac{1}{2}(A(n) - |A(n)|) \in \mathbb{R}^{n^{\text{c}} \times n^{\text{c}}}$ imposes inflow states, $u^0 \in L^2(\Omega)$ is the initial condition, and T is the final time. As discussed in the Introduction, one of the advantages — and in fact a design criterion for the numerical flux — of the DG method is the energy stability for hyperbolic systems and convection-dominated systems. Specifically, the solution u_h associated with the

DG discretization of (29) satisfies

$$\frac{d}{dt}\|u_h\|^2_{L^2(\Omega)} \leq -\sum_{\sigma\in\Sigma_h^{\mathrm{b}}} 2\int_\sigma u_h^+ \cdot A(n^+)^- u^{\mathrm{b}} ds; \tag{30}$$

in words, the energy, defined as $\|u_h\|^2_{L^2(\Omega)}$, enters the system only through the boundary, and no spurious energy is created by the discretization (see, e.g., [7]). The energy stability is an important property even for steady-state calculations, as the solution is obtained through the PTC procedure describe in Section 2.4.

We now show that the DG-RB-EQP formulation of (29) is also energy stable for any EQP weights $\{\rho_\kappa^\nu \in \mathbb{R}_{\geq 0}\}_{\kappa\in\mathcal{T}_h}$. The semi-discrete form associated with the DG-RB-EQP spatial discretization of the linear hyperbolic system (29) is as follows: find $u_N^\nu(t) \in \mathcal{V}_N$, $t \in (0,T]$, such that

$$\sum_{\kappa\in\mathcal{T}_h} \rho_\kappa^\nu \int_\kappa v \cdot \left.\frac{\partial u_N^\nu}{\partial t}\right|_t dx + r^\nu(u_N^\nu(t), v) = \sum_{\kappa\in\mathcal{T}_h} \rho_\kappa^\nu \left(\int_\kappa v \cdot \left.\frac{\partial u_N^\nu}{\partial t}\right|_t dx + \eta_\kappa^{\mathrm{c}}(u_N^\nu(t), v)\right) = 0 \quad \forall v \in \mathcal{V}_N. \tag{31}$$

The elemental residual form $\eta_\kappa^c(\cdot,\cdot)$ given in (16) is fully described by the the convection flux $F(w) = Aw$, the upwinded interior numerical flux $\hat{F}(w^+, w^-; n^+) = \frac{1}{2}(A(n^+)w^+ + A(n^+)w^-) + \frac{1}{2}|A(n^+)|[w]_-^+$, where $|\cdot|$ denotes the matrix absolute value, and the upwinded boundary numerical flux $\hat{F}^{\mathrm{b}}(w^+; n^+) = \hat{F}(w^+, u^{\mathrm{b}}; n^+)$. We have the following energy-stability statement.

Proposition 1 (energy stability for linear hyperbolic systems) *For any EQP weights $\{\rho_\kappa^\nu \in \mathbb{R}_{\geq 0}\}_{\kappa\in\mathcal{T}_h}$, the solution u_N^ν to the DG-RB-EQP problem* (31) *associated with the linear hyperoblic system* (29) *is energy stable (modulo inflow data u^{b}) with the following energy balance:*

$$\begin{aligned}\frac{d}{dt}\left(\sum_{\kappa\in\mathcal{T}_h} \rho_\kappa^\nu \|u_N^\nu\|^2_{L^2(\kappa)}\right) + \sum_{\kappa\in\mathcal{T}_h} \rho_\kappa^\nu \left(\sum_{\sigma\in\partial\kappa\cap\Sigma_h^{\mathrm{i}}} \frac{1}{2}\int_\sigma [u_N^\nu]_-^+ \cdot |A(n^+)|[u_N^\nu]_-^+ ds + \sum_{\sigma\in\partial\kappa\cap\Sigma_h^{\mathrm{b}}} \int_\sigma {u_N^\nu}^+ \cdot |A(n^+)| {u_N^\nu}^+ ds\right)\\ = -\sum_{\kappa\in\mathcal{T}_h} \rho_\kappa^\nu \sum_{\sigma\in\partial\kappa\cap\Sigma_h^{\mathrm{b}}} 2\int_\sigma {u_N^\nu}^+ \cdot A(n^+)^- u^{\mathrm{b}} ds.\end{aligned} \tag{32}$$

Consequently,

$$\frac{d}{dt}\left(\sum_{\kappa\in\mathcal{T}_h} \rho_\kappa^\nu \|u_N^\nu\|^2_{L^2(\kappa)}\right) \leq -\sum_{\kappa\in\mathcal{T}_h} \rho_\kappa^\nu \sum_{\sigma\in\partial\kappa\cap\Sigma_h^{\mathrm{b}}} 2\int_\sigma {u_N^\nu}^+ \cdot A(n^+)^- u^{\mathrm{b}} ds. \tag{33}$$

In words, no spurious energy is created by the discretization.

Proof *We analyze the energy stability of the element-wise decomposed convection residual* (16)*. To this end, we first note that, by integration parts and the symmetry of A (i.e., $A_{ikj} = A_{jki}$ for $i,j = 1,\ldots,n^{\mathrm{c}}$),*

$$\begin{aligned} r_\kappa^{\mathrm{c,e}}(v,v) &= -\int_\kappa \nabla v : Av dx = \sum_{k=1}^d \sum_{i,j=1}^{n^{\mathrm{c}}} \left(-\int_\kappa \frac{\partial v_i}{\partial x_k} A_{ikj} v_j dx\right)\\ &= \sum_{k=1}^d \sum_{i,j=1}^{n^{\mathrm{c}}} \left(-\frac{1}{2}\int_\kappa \frac{\partial v_i}{\partial x_k} A_{ikj} v_j dx + \frac{1}{2}\int_\kappa v_i A_{ikj} \frac{\partial v_j}{\partial x_k} dx - \frac{1}{2}\sum_{\sigma\in\partial\kappa}\int_\sigma v_i^\pm n_k^\pm A_{ikj} v_j^\pm ds\right)\\ &= -\frac{1}{2}\sum_{\sigma\in\partial\kappa}\int_\sigma v^\pm \cdot A(n^\pm) v^\pm ds, \end{aligned}$$

where $+$ (resp. $-$) is chosen for the element κ^+ (resp. κ^-) of the facet σ. It hence follows that

$$\begin{aligned}\eta_\kappa^{\mathrm{c}}(v,v) &= r_\kappa^{\mathrm{c,e}}(v,v) + \sum_{\sigma\in\partial\kappa\cap\Sigma_h^{\mathrm{i}}} r_{\sigma,\kappa}^{\mathrm{c,f,split}}(v,v) + \sum_{\sigma\in\partial\kappa\cap\Sigma_h^{\mathrm{b}}} r_\sigma^{\mathrm{c,f}}(v,v)\\ &= \sum_{\sigma\in\partial\kappa\cap\Sigma_h^{\mathrm{i}}} \int_\sigma \left(-\frac{1}{2}v^\pm \cdot A(n^\pm)v^\pm + \frac{1}{4}[v\cdot A(n)v]_\mp^\pm + \frac{1}{2}[v]_-^+ \cdot \hat{F}(v^+, v^-; n^+)\right) ds\\ &\quad + \sum_{\sigma\in\partial\kappa\cap\Sigma_h^{\mathrm{b}}} \int_\sigma \left(-\frac{1}{2}v^+ \cdot A(n^+)v^+ + v^+ \cdot \hat{F}^{\mathrm{b}}(v^+; n^+)\right) ds\end{aligned}$$

A tedious but straightforward algebraic manipulation simplifies the integrand over the interior facet $\sigma \in \partial\kappa \cap \Sigma_h^{\mathrm{i}}$ *to*

$$-\frac{1}{2}v^{\pm}\cdot A(n^{\pm})v^{\pm}+\frac{1}{4}[v\cdot A(n)v]^{\pm}_{\mp}+\frac{1}{2}[v]^{+}_{-}\cdot(\frac{1}{2}A(n^{+})v^{+}+\frac{1}{2}A(n^{+})v^{-}+\frac{1}{2}|A(n^{+})|[v]^{+}_{-})=\frac{1}{4}[v]^{+}_{-}\cdot|A(n^{+})|[v]^{+}_{-},$$

where we have used the definition of the interior numerical flux $\hat{F}$ *and the fact that* $n^{+}=-n^{-}$ *and hence* $A(n^{+})=-A(n^{-})$*. A similar manipulation simplifies the integrand over the boundary facet* $\sigma\in\partial\kappa\cap\Sigma_h^{\mathrm{b}}$ *to*

$$\begin{aligned}&-\frac{1}{2}v^{+}\cdot A(n^{+})v^{+}+\frac{1}{2}v^{+}\cdot A(n^{+})v^{+}+\frac{1}{2}v^{+}\cdot A(n^{+})u^{\mathrm{b}}+\frac{1}{2}v^{+}\cdot|A(n^{+})|(v^{+}-u^{\mathrm{b}})\\&\quad=\frac{1}{2}v^{+}\cdot|A(n^{+})|v^{+}+\frac{1}{2}v^{+}\cdot(A(n^{+})-|A(n^{+})|)u^{b}=\frac{1}{2}v^{+}\cdot|A(n^{+})|v^{+}+v^{+}\cdot A(n^{+})^{-}u^{b},\end{aligned}$$

where we have used the definition of the boundary numerical flux $\hat{F}^{\mathrm{b}}$ *and the inflow flux matrix* $(n^{+}\cdot A)^{-}$*. We hence conclude that the elemental residual form is non-negative in the sense that*

$$\eta_{\kappa}^{\mathrm{c}}(v,v)=\sum_{\sigma\in\partial\kappa\cap\Sigma_h^{\mathrm{i}}}\frac{1}{4}\int_{\sigma}[v]^{+}_{-}\cdot|A(n^{+})|[v]^{+}_{-}ds+\sum_{\sigma\in\partial\kappa\cap\Sigma_h^{\mathrm{b}}}\int_{\sigma}\left(\frac{1}{2}v^{+}|A(n^{+})|v^{+}+v^{+}A(n^{+})^{-}u^{b}\right)ds. \quad (34)$$

On the other hand, we note that

$$\int_{\kappa}v\cdot\frac{\partial v}{\partial t}dx=\frac{1}{2}\frac{d}{dt}\|v\|^{2}_{L^{2}(\kappa)}. \quad (35)$$

The substitution of (34) *and* (35) *to* (31) *yields the energy balance statement* (32)*. We then note that the second term of* (32) *is non-negative to obtain the energy stability statement* (33)*.*

We make a few remarks on Proposition 1.

Remark 1 If we had naively decomposed the convection residual as $r_h^{\mathrm{c}}(w,v)=\sum_{\kappa\in\mathcal{T}_h}r_h^{\mathrm{c}}(w,v|_{\kappa})$, then the elemental residuals would not be element-wise energy stable when applied to the linear hyperbolic system (29). The associated EQP approximation hence would not be energy stable in general.

Remark 2 Due to the particular form of the (split) interior facet residual form $r_{\sigma,\kappa}^{\mathrm{c,f,split}}(\cdot,\cdot)$ defined by (17), the DG-RB-EQP formulation inherits the energy stability (30) for the DG formulation for *any* set of EQP weights. We emphasize that the energy stability is preserved independent of the tolerance used in EQP $\mathtt{LP}_N^{\nu}$.

Remark 3 The energy stability can be shown for more general forms of interior numerical fluxes that provide dissipation in the sense that $[w]^{+}_{-}\cdot\left(\hat{F}(w^{+},w^{-};n^{+})-n^{+}\cdot\frac{1}{2}(F(w^{+})+F(w^{-}))\right)\geq 0\ \forall w^{+},w^{-}\in\mathbb{R}^{n^{\mathrm{c}}}$. This generalization includes fluxes such as the Lax-Friedrichs flux.

Remark 4 If all EQP weights ρ^{ν} are set to unity, then the DG-RB-EQP energy stability statement (32) is identical to the DG energy statement (30); this is a direct consequence of the fact that the element-wise residual $\eta_{\kappa}^{\mathrm{c}}(\cdot,\cdot)$ in the DG-RB-EQP formulation is a proper decomposition of the DG residual.

4.2 Symmetry and non-negativity for diffusion systems

We next consider the application of the DG-RB-EQP formulation to a (steady) linear diffusion system

$$\begin{aligned}-\nabla\cdot(K\nabla u)&=0\quad\text{in }\Omega,\\ u&=u^{\mathrm{b}}\quad\text{on }\partial\Omega,\end{aligned} \quad (36)$$

where $K\in\mathbb{R}^{n^{\mathrm{c}}\times d\times n^{\mathrm{c}}\times d}$ is an order-4 tensor that is symmetric (i.e., $K_{ikjl}=K_{jkil}$) and satisfies the ellipticity condition (i.e., $\xi:K\xi>0$ for all $\xi\in\mathbb{R}^{n^{\mathrm{c}}\times d}$ such that $\xi\neq 0$). The bilinear form associated with the weak formulation of (36) is symmetric and non-negative, and so are the bilinear forms associated with many finite element discretizations including the BR2 DG discretization [3]. As discussed in the Introduction, preserving the symmetry and non-negativity of diffusive systems, which also arise in

structural mechanics, was a focus of the recent hyperreduction works in [15] and [12]. (For simplicity, we here consider a (pure) Dirichlet problem; however, both the symmetry and non-negativity analyses readily extend to mixed problems with Dirichlet and Neumann boundary conditions.)

We now show that the bilinear form for the DG-RB-EQP formulation of (36) is also symmetric and non-negative. The DG-RB-EQP formulation of (36) is as follows: find $u_N^\nu \in \mathcal{V}_N$ such that

$$r^\nu(u_N^\nu, v) \equiv \sum_{\kappa\in\mathcal{T}_h} \rho_\kappa^\nu \eta_\kappa^{\mathrm{d}}(u_N^\nu, v) = 0 \quad \forall v \in \mathcal{V}_N. \tag{37}$$

The bilinear form associated with this linear problem is the Jacobian form

$$r^{\nu\prime}(\cdot; w, v) = \sum_{\kappa\in\mathcal{T}_h} \rho_\kappa^\nu \eta_\kappa^{\mathrm{d}\prime}(\cdot; w, v). \tag{38}$$

(The Jacobian form $r^{\nu\prime}(\cdot;\cdot,\cdot)$ is independent of the first argument (i.e., the linearization point) since the residual form $r^\nu(\cdot,\cdot)$ is affine in the first argument for a linear problem.) We will show $r^{\nu\prime}(\cdot; w, v)$ is symmetric and non-negative with respect to w and $v \in \mathcal{V}_h$. The symmetry and non-negativity of the Jacobian form implies the symmetry and non-negativity of the (algebraic) Jacobian $J_N^\nu \in \mathbb{R}^{n^{\mathrm{c}}\times n^{\mathrm{c}}}$ given in (22) because $(J_N^\nu)_{ij} = r^{\nu\prime}(\cdot;\phi_j,\phi_i)$, $i,j = 1,\ldots,N$.

To facilitate the analysis of the Jacobian form (38), we introduce the boundary lifting operator associated with the homogeneous Dirichlet boundary condition: $\ell_\sigma^{\mathrm{b},0}(w^+) \in (\mathcal{V}_h)^d$ that has the support over κ^+ and satisfies

$$\int_{\kappa^+} v : \ell_\sigma^{\mathrm{b},0}(w^+) dx = -\int_\sigma v : (w^+ \otimes n^+) ds, \quad \forall v \in (\mathcal{V}_h)^d. \tag{39}$$

Due to the linearity of the lifting operator, the lifting operator (12) for inhomogneous Dirichlet boundary condition can be expressed in terms of the homogeneous counterpart (39) as $\ell_\sigma^{\mathrm{b}}(w^+) = \ell_\sigma^{\mathrm{b},0}(w^+) - \ell_\sigma^{\mathrm{b},0}(u^{\mathrm{b}})$. We in addition introduce an element-wise (rather than facet-wise) lifting operator [3],

$$L_\kappa(v) \equiv \sum_{\sigma\in\partial\kappa\cap\Sigma_h^{\mathrm{i}}} \ell_\sigma(\llbracket v \rrbracket) + \sum_{\sigma\in\partial\kappa\cap\Sigma_h^{\mathrm{b}}} \ell_\sigma^{\mathrm{b},0}(v^+).$$

We now prove the symmetry of $r^{\nu\prime}(\cdot; w, v)$ with respect to w and v.

Proposition 2 (symmetry of the Jacobian for diffusion systems) *For any EQP weights $\{\rho_\kappa^\nu \in \mathbb{R}_{\geq 0}\}_{\kappa\in\mathcal{T}_h}$, the Jacobian form (38) associated with the linear diffusion system (36) is symmetric in the sense that*

$$r^{\nu\prime}(\cdot; w, v) = r^{\nu\prime}(\cdot; v, w) \quad \forall w, v \in \mathcal{V}_h.$$

Proof It suffices to show that the Jacobian form for the elemental residual (18), $\eta_\kappa^{\mathrm{d}\prime}(\cdot,\cdot) = r_\kappa^{\mathrm{d,e}\prime}(\cdot,\cdot) + \sum_{\sigma\in\partial\kappa\cap\Sigma_h^{\mathrm{i}}} r_{\sigma,\kappa}^{\mathrm{d,f,split}\prime}(\cdot,\cdot) + \sum_{\sigma\in\partial\kappa\cap\Sigma_h^{\mathrm{b}}} r_\sigma^{\mathrm{d,f}\prime}(\cdot,\cdot)$, is symmetric. The symmetry of $r_\kappa^{\mathrm{d,e}\prime}(\cdot,\cdot)$ is obvious from the definition (8). The symmetry of the interior facet Jacobian form $r_{\sigma,\kappa}^{\mathrm{d,f,split}\prime}(\cdot,\cdot)$, $\sigma \in \Sigma_h^{\mathrm{i}}$, follows from the definition of the interior lifting operator (11): for $\sigma \in \Sigma_h^{\mathrm{i}}$,

$$\begin{aligned} r_{\sigma,\kappa^\pm}^{\mathrm{d,f,split}\prime}(\cdot; w, v) &\equiv -\int_\sigma \left(\frac{1}{2}\nabla v^\pm : K\llbracket w \rrbracket + \frac{1}{2}\llbracket v \rrbracket : K(\nabla w^\pm + \theta_\sigma \ell_\sigma^\pm(\llbracket w \rrbracket))\right) ds \\ &= -\int_\sigma \left(\frac{1}{2}\nabla v^\pm : K\llbracket w \rrbracket + \frac{1}{2}\llbracket v \rrbracket : K\nabla w^\pm\right) ds + \theta_\sigma \int_{\kappa^\pm} \ell_\sigma(\llbracket v \rrbracket) : K\ell_\sigma(\llbracket w \rrbracket) dx; \end{aligned}$$

we readily observe that the form is symmetric. Similarly, the symmetry of the boundary facet Jacobian form $r_\sigma^{\mathrm{d,f}\prime}(\cdot,\cdot)$, $\sigma \in \Sigma_h^{\mathrm{b}}$, follows from the definition of the boundary lifting operator (39): for $\sigma \in \Sigma_h^{\mathrm{b}}$,

$$\begin{aligned} r_\sigma^{\mathrm{d,f}\prime}(\cdot; w, v) &\equiv -\int_\sigma \Big(\nabla v^+ : K(w^+ \otimes n^+) + (v^+ \otimes n^+) : K(\nabla w^+ + \theta_\sigma \ell_\sigma^{\mathrm{b},0}(w^+; \mu))\Big) ds \\ &= -\int_\sigma \Big(\nabla v^+ : K(w^+ \otimes n^+) + (v^+ \otimes n^+) : K\nabla w^+\Big) ds + \theta_\sigma \int_\kappa \ell_\sigma^{\mathrm{b},0}(v^+) : K\ell_\sigma^{\mathrm{b},0}(w^+) dx; \end{aligned}$$

we again observe that the form is symmetric. Since each Jacobian form that comprises $\eta_\kappa^{\mathrm{d}\prime}(\cdot,\cdot)$ is symmetric, the elemental Jacobian form $\eta_\kappa^{\mathrm{d}\prime}(\cdot,\cdot)$ is symmetric. It follows that the EQP Jacobian form $r^{\nu\prime}(\cdot;\cdot,\cdot)$, which results from a sum of elemental Jacobian forms $\eta_\kappa^{\mathrm{d}\prime}$, is symmetric.

Before we prove the non-negativity of the Jacobian form $r^{\nu\prime}(\cdot; v, v)$ with respect to $v \in \mathcal{V}_h$, we provide the following lemma.

Lemma 1 *The elemental residual for the linear diffusion system* (36) *satisfies*

$$\begin{aligned}\eta_\kappa^{\mathrm{d}}(v,v) = \int_\kappa (\nabla v + L_\kappa(v)) : K(\nabla v + L_\kappa(v)) dx + \Big[- \int_\kappa L_\kappa(v) : K L_\kappa(v) dx \\ + \sum_{\sigma \in \partial\kappa \cap \Sigma_h^{\mathrm{i}}} \theta_\sigma \int_\kappa \ell_\sigma([\![v]\!]) : K \ell_\sigma([\![v]\!]) dx + \sum_{\sigma \in \partial\kappa \cap \Sigma_h^{\mathrm{b}}} \theta_\sigma \int_\kappa \ell_\sigma^{\mathrm{b}}(v^+) : K \ell_\sigma^{\mathrm{b}}(v^+) dx \Big] \\ + \sum_{\sigma \in \partial\kappa \cap \Sigma_h^{\mathrm{b}}} \int_\sigma \left(\nabla v^+ : K(u^{\mathrm{b}} \otimes n^+) + (v^+ \otimes n^+) : K \theta_\sigma \ell_\sigma^{\mathrm{b},0}(u^{\mathrm{b}}) \right) ds.\end{aligned} \tag{40}$$

Consequently,

$$\eta_\kappa^{\mathrm{d}}(v,v) \geq \sum_{\sigma \in \partial\kappa \cap \Sigma_h^{\mathrm{b}}} \int_\sigma \left(\nabla v^+ : K(u^{\mathrm{b}} \otimes n^+) + (v^+ \otimes n^+) : K \theta_\sigma \ell_\sigma^{\mathrm{b},0}(u^{\mathrm{b}}) \right) ds. \tag{41}$$

Proof A direct manipulation of the elemental residual form yields

$$\begin{aligned}\eta_\kappa^{\mathrm{d}}(v,v) &= r_\kappa^{\mathrm{d,e}}(v,v) + \sum_{\sigma \in \partial\kappa \cap \Sigma_h^{\mathrm{i}}} r_{\sigma,\kappa^\pm}^{\mathrm{d,f,split}}(v,v) + \sum_{\sigma \in \partial\kappa \cap \Sigma_h^{\mathrm{b}}} r_\sigma^{\mathrm{d,f}}(v,v) \\ &= \int_\kappa \nabla v : K \nabla v dx - \sum_{\sigma \in \partial\kappa \cap \Sigma_h^{\mathrm{i}}} \int_\sigma \left(\frac{1}{2} \nabla v^\pm : K [\![v]\!] + \frac{1}{2} [\![v]\!] : K (\nabla v^\pm + \theta_\sigma \ell_{\sigma,j}^\pm([\![v]\!])) \right) ds \\ &\quad - \sum_{\sigma \in \partial\kappa \cap \Sigma_h^{\mathrm{b}}} \int_\sigma \left(\nabla v^+ : K((v^+ - u^{\mathrm{b}}) \otimes n^+) + (v^+ \otimes n^+) : K(\nabla v^+ + \theta_\sigma \ell_\sigma^{\mathrm{b},0}(v^+) - \theta_\sigma \ell_\sigma^{\mathrm{b},0}(u^{\mathrm{b}})) \right) ds \\ &= \int_\kappa \nabla v : K \nabla v dx + \sum_{\sigma \in \partial\kappa \cap \Sigma_h^{\mathrm{i}}} \int_\kappa \left(\nabla v : K \ell_\sigma([\![v]\!]) + \ell_\sigma([\![v]\!]) : K(\nabla v + \theta_\sigma \ell_\sigma([\![v]\!])) \right) dx \\ &\quad + \sum_{\sigma \in \partial\kappa \cap \Sigma_h^{\mathrm{b}}} \int_\kappa \left(\nabla v : K \ell_\sigma^{\mathrm{b},0}(v^+) + \ell_\sigma^{\mathrm{b},0}(v^+) : K(\nabla v + \theta_\sigma \ell_\sigma^{\mathrm{b},0}(v^+)) \right) dx \\ &\quad + \sum_{\sigma \in \partial\kappa \cap \Sigma_h^{\mathrm{b}}} \int_\sigma \left(\nabla v^+ : K(u^{\mathrm{b}} \otimes n^+) + (v^+ \otimes n^+) : K \theta_\sigma \ell_\sigma^{\mathrm{b},0}(u^{\mathrm{b}}) \right) ds \\ &= \int_\kappa (\nabla v + L_\kappa(v)) : K(\nabla v + L_\kappa(v)) dx + \Big[- \int_\kappa L_\kappa(v) : K L_\kappa(v) dx \\ &\quad + \sum_{\sigma \in \partial\kappa \cap \Sigma_h^{\mathrm{i}}} \theta_\sigma \int_\kappa \ell_\sigma([\![v]\!]) : K \ell_\sigma([\![v]\!]) + \sum_{\sigma \in \partial\kappa \cap \Sigma_h^{\mathrm{b}}} \theta_\sigma \int_\kappa \ell_\sigma^{\mathrm{b},0}(v^+) : K \ell_\sigma^{\mathrm{b},0}(v^+) \Big] \\ &\quad + \sum_{\sigma \in \partial\kappa \cap \Sigma_h^{\mathrm{b}}} \int_\sigma \left(\nabla v^+ : K(u^{\mathrm{b}} \otimes n^+) + (v^+ \otimes n^+) : K \theta_\sigma \ell_\sigma^{\mathrm{b},0}(u^{\mathrm{b}}) \right) ds;\end{aligned}$$

here the first equality follows from the definition of the residual forms and the relationship between the homogeneous and inhomogeneous boundary lifting operators, the second equality follows from the definition of the lifting operators, and the last equality follows from simple algebraic manipulations, proving (40).

We now prove (41). *We readily observe that the first term of* (40) *is non-negative because it is quadratic and* K *is elliptic. We wish to show that the term in the bracket in* (40) *is non-negative. For notational convenience, we introduce*

$$\ell_\sigma^\bullet(v) \equiv \begin{cases} \ell_\sigma([\![v]\!]), & \sigma \in \Sigma_h^{\mathrm{i}} \\ \ell_\sigma^{\mathrm{b},0}(v^+), & \sigma \in \Sigma_h^{\mathrm{b}} \end{cases}.$$

With this notation the element lifting operator can be written concisely as $L_\kappa(v) \equiv \sum_{\sigma\in\partial\kappa} \ell^\bullet_\sigma(v)$. *We then observe that*

$$\begin{aligned}\int_\kappa L_\kappa(v) : KL_\kappa(v)dx &= \int_\kappa \Big(\sum_{\sigma\in\partial\kappa} \ell^\bullet_\sigma(v)\Big) : K\Big(\sum_{\sigma'\in\partial\kappa} \ell^\bullet_{\sigma'}(v)\Big)dx = \sum_{\sigma\in\partial\kappa}\sum_{\sigma'\in\partial\kappa}\int_\kappa \ell^\bullet_\sigma(v) : K\ell^\bullet_{\sigma'}(v)dx \\ &\le \sum_{\sigma\in\partial\kappa}\sum_{\sigma'\in\partial\kappa}\Big(\int_\kappa \ell^\bullet_\sigma(v) : K\ell^\bullet_\sigma(v)dx\Big)^{1/2}\Big(\int_\kappa \ell^\bullet_{\sigma'}(v) : K\ell^\bullet_{\sigma'}(v)dx\Big)^{1/2} \\ &\le \sum_{\sigma\in\partial\kappa}\sum_{\sigma'\in\partial\kappa}\int_\kappa \ell^\bullet_\sigma(v) : K\ell^\bullet_\sigma(v)dx \le \sum_{\sigma\in\partial\kappa}\theta_\sigma\int_\kappa \ell^\bullet_\sigma(v) : K\ell^\bullet_\sigma(v)dx;\end{aligned}$$

here, the first inequality follows from the Cauchy-Schwarz inequality (which applies since K *is elliptic), the second inequality follows from the Young's inequality, and the last inequality follows from the fact that* θ_σ *is greater than the number of facet on* κ *(as we specified in Section 2.3). We hence observe that the term in the bracket in* (40) *satisfies*

$$\begin{aligned}&\Big[-\int_\kappa L_\kappa(v) : KL_\kappa(v)dx + \sum_{\sigma\in\partial\kappa}\theta_\sigma\int_\kappa \ell^\bullet_\sigma(v) : K\ell^\bullet_\sigma(v)dx\Big] \\ &\ge -\sum_{\sigma\in\partial\kappa}\theta_\sigma\int_\kappa \ell^\bullet_\sigma(v) : K\ell^\bullet_\sigma(v)dx + \sum_{\sigma\in\partial\kappa}\theta_\sigma\int_\kappa \ell^\bullet_\sigma(v) : K\ell^\bullet_\sigma(v)dx \ge 0;\end{aligned}$$

the term in the bracket in (40) *is non-negative. As both the first term and the term in the bracket in* (40) *are non-negative, we conclude that* (40) *implies* (41).

Proposition 3 (non-negativity of the Jacobian for diffusion systems) *For any EQP weights* $\{\rho^\nu_\kappa \in \mathbb{R}_{\ge 0}\}_{\kappa\in\mathcal{T}_h}$, *the Jacobian form* (38) *associated with the linear diffusion system* (36) *is non-negative in the sense that*

$$r^{\nu\prime}(\cdot; v, v) \ge 0 \quad \forall v \in \mathcal{V}_h.$$

Proof It suffices to show that the elemental Jacobian form $\eta^{\mathrm{d}\prime}_\kappa(\cdot; v, v)$ *is non-negative with respect to* $v \in \mathcal{V}_h$. *The linearization of the form* (40) *in Lemma 1 yields*

$$\begin{aligned}\eta^{\mathrm{d}\prime}_\kappa(\cdot; v, v) = &\int_\kappa (\nabla v + L_\kappa(v)) : K(\nabla v + L_\kappa(v))dx + \Big[-\int_\kappa L_\kappa(v) : KL_\kappa(v)dx \\ &+ \sum_{\sigma\in\partial\kappa\cap\Sigma^{\mathrm{i}}_h}\theta_\sigma\int_\kappa \ell_\sigma([\![v]\!]) : K\ell_\sigma([\![v]\!]) + \sum_{\sigma\in\partial\kappa\cap\Sigma^{\mathrm{b}}_h}\theta_\sigma\int_\kappa \ell^{\mathrm{b},0}_\sigma(v^+) : K\ell^{\mathrm{b},0}_\sigma(v^+)\Big].\end{aligned}$$

As in the proof of Lemma 1, the term in the bracket is non-negative if θ_σ *is greater than the number of facet on* κ *(as we specified in Section 2.3). We hence conclude that* $\eta^{\mathrm{d}\prime}_\kappa(\cdot; v, v) \ge 0$. *The summation of the elemental Jacobians form according to* (38) *yields the desired result.*

We make a few remarks on Propositions 2 and 3, which are the counterpart of the earlier remarks on Proposition 1.

Remark 5 If we had naively decomposed the diffusion residual as $r^{\mathrm{d}}_h(w, v) = \sum_{\kappa\in\mathcal{T}_h} r^{\mathrm{d}}_h(w, v|_\kappa)$, then the elemental residuals would be neither symmetric nor non-negative when applied to the linear diffusion system (36). The associated EQP approximation hence would be neither symmetric nor non-negative in general.

Remark 6 Due to the particular form of the (split) interior facet residual form $r^{\mathrm{d,f,split}}_{\sigma,\kappa}(\cdot,\cdot)$ defined by (19), the DG-RB-EQP formulation inherits the symmetry and non-negativity of the Jacobian form for the DG formulation for *any* set of EQP weights. We emphasize that the symmetry and non-negativity are preserved independent of the tolerance used in the EQP $\mathtt{LP}^\nu_N$.

4.3 Energy stability for convection-diffusion systems

We now consider the application of the DG-RB-EQP formulation to a convection-diffusion system

$$\begin{aligned}\frac{\partial u}{\partial t} + \nabla \cdot (Au) - \nabla \cdot (K \nabla u) = 0 \quad &\text{in } \Omega \times (0,T],\\ u = u^{\mathrm{b}} \quad &\text{on } \partial\Omega \times (0,T],\\ u(t=0) = u^0 \quad &\text{in } \Omega \times \{0\},\end{aligned}$$

where, as considered in problems (29) and (36), $A \in \mathbb{R}^{n^{\mathrm{c}} \times d \times n^{\mathrm{c}}}$ is symmetric (i.e., $A_{ikj} = A_{jki}$), and $K \in \mathbb{R}^{n^{\mathrm{c}} \times d \times n^{\mathrm{c}} \times d}$ is symmetric (i.e., $K_{ikjl} = K_{jkil}$) and satisfies the ellipticity condition (i.e., $\xi : K\xi > 0$ for all $\xi \in \mathbb{R}^{n^{\mathrm{c}} \times d}$ such that $\xi \neq 0$).

The semi-discrete form associated with the DG-RB-EQP spatial discretization of the problem is as follows: find $u(t) \in \mathcal{V}_N$, $t \in (0,T]$, such that

$$\sum_{\kappa \in \mathcal{T}_h} \rho_\kappa^\nu \left(\int_\kappa v \cdot \left. \frac{\partial u}{\partial t} \right|_t dt + \eta_\kappa^{\mathrm{c}}(u(t), v) + \eta_\kappa^{\mathrm{d}}(u(t), v) \right) = 0 \quad \forall v \in \mathcal{V}_N, \tag{42}$$

where $\eta_\kappa^{\mathrm{c}}(\cdot,\cdot)$ and $\eta_\kappa^{\mathrm{d}}(\cdot,\cdot)$ are identical to the element-wise convection and diffusion residual forms for (31) and (37), respectively. We have the following energy stability statement.

Proposition 4 (energy stability for linear convection-diffusion systems) *For any EQP weights $\{\rho_\kappa^\nu \in \mathbb{R}_{\geq 0}\}_{\kappa \in \mathcal{T}_h}$, the DG-RB-EQP formulation applied to* (42) *is energy stable (modulo boundary data u^{b}) in the sense that*

$$\begin{aligned}&\frac{d}{dt}\left(\sum_{\kappa \in \mathcal{T}_h} \rho_\kappa^\nu \|u\|_{L^2(\kappa)}^2 \right)\\ &\leq - \sum_{\kappa \in \mathcal{T}_h} \rho_\kappa^\nu \sum_{\sigma \in \partial\kappa \cap \Sigma_h^{\mathrm{b}}} 2 \int_\sigma \left(u^+ \cdot A(n^+)^- u^b + \nabla u^+ : K(u^{\mathrm{b}} \otimes n^+) + (u^+ \otimes n^+) : K\theta_\sigma \ell_\sigma^{\mathrm{b},0}(u^{\mathrm{b}}) \right) ds.\end{aligned}$$

In words, no spurious energy is created by the discretization.

Proof *The proof is a direct consequence of the stability of the DG-RB-EQP discretization for hyperbolic systems in Proposition 1 and the non-negativity of the discretization for diffusion systems in Proposition 3 and in particular* (41) *in Lemma 1.*

4.4 *A priori* error estimates

In Sections 4.1 through 4.3, we analyzed the stability of the DG-RB-EQP discretization for linear hyperbolic and convection-diffusion systems. We now analyze the error between the RB solution (20) and the RB-EQP solution (25), $\|u_N - u_N^\nu\|_{\mathcal{V}_h}$, using two approaches. The first analysis builds on the Brezzi-Rappaz-Raviart (BRR) theorem [9], provides conditions under which the RB-EQP solution exists, and provides a bound of the error. This BRR error bound was originally presented in [39] in the context of continuous Galerkin method; we here reproduce the result for completeness.

Proposition 5 (Brezzi-Rappaz-Raviart error bound (Proposition 3.2 in [39])) *For a fixed $\mu \in \mathcal{D}$, we introduce $\hat{\mathbf{u}}_N \in \mathbb{R}^N$ such that*

$$\|\mathbf{u}_N - \hat{\mathbf{u}}_N\|_2 \leq \delta_T \tag{43}$$

for some $\delta_T \in \mathbb{R}_{\geq 0}$ and such that $\mathbf{J}_N(\hat{\mathbf{u}}_N)$ is non-singular. Suppose

$$\|\mathbf{J}_N(\hat{\mathbf{u}}_N)^{-1} \mathbf{r}_N^\nu(\hat{\mathbf{u}}_N)\|_\infty \leq \delta_R \tag{44}$$

$$\|\mathbf{J}_N(\hat{\mathbf{u}}_N)^{-1} \mathbf{J}_N^\nu(\hat{\mathbf{u}}_N) - I\|_{\max} \leq \delta_J \tag{45}$$

for some $\delta_R \in \mathbb{R}_{\geq 0}$ and $\delta_J \in [0, 1/N)$; here, for any $A \in \mathbb{R}^{N \times N}$, $\|A\|_{\max} \equiv \max_{i,j} |A_{ij}|$. We in addition define $L(\alpha) \equiv 2 \sup_{\mathbf{w} \in \bar{B}(\mathbf{u}_N, \alpha)} \|\mathbf{J}_N(\hat{\mathbf{u}}_N)^{-1} \mathbf{J}_N^\nu(\mathbf{w}) - I\|_2$. Suppose $L(2\sqrt{N}\delta_R/(1 - N\delta_J)) \leq (1 - N\delta_J)/2$.

Then, for all $\beta \geq 2\sqrt{N}\delta_R/(1-N\delta_J)$ such that $L(\beta) \leq 1-N\delta_J$, there exists a unique solution $\mathbf{u}_N^\nu \in \mathbb{R}^N$ to (25) in the ball $\bar{B}(\hat{\mathbf{u}}_N, \beta)$. Moreover,

$$\|u_N - u_N^\nu\|_{\mathcal{V}_h} = \|\mathbf{u}_N - \mathbf{u}_N^\nu\|_2 \leq \frac{2\sqrt{N}\delta_R}{1-N\delta_J} + \delta_T \tag{46}$$

Proof See Proposition 3.2 in [39].

The BRR analysis in Proposition 5 identifies a sufficient condition for the solution to the RB-EQP problem (25) to exist; it also provides an error bound for $\|u_N - u_N^\nu\|_{\mathcal{V}_h}$. However, this BRR error bound is not asymptotically sharp. Here we provide an alternative analysis which provides an asymptotically sharper error estimate.

Proposition 6 (asymptotic error estimate) *Suppose the following assumptions hold: (i) the training condition (43) and the Jacobian condition (45) (but not the residual condition (44)) of the BRR error bound in Proposition 5 are satisfied; (ii) a residual condition*

$$\|\mathbf{J}_N(\hat{\mathbf{u}}_N)^{-1}(\mathbf{r}_N(\hat{\mathbf{u}}_N) - \mathbf{r}_N^\nu(\hat{\mathbf{u}}_N))\|_\infty \leq \delta_R \tag{47}$$

for some $\delta_R \in \mathbb{R}_{\geq 0}$ is satisfied; (iii) the conditions for the existence of the unique solution $\mathbf{u}_N^\nu \in \mathbb{R}^N$ in Proposition 5 are satisfied; and (iv) the residual $\mathbf{r}_N : \mathbb{R}^N \to \mathbb{R}^N$ and $\mathbf{r}_N^\nu : \mathbb{R}^N \to \mathbb{R}^N$ are thrice differentiable. Then

$$\|u_N - u_N^\nu\|_{\mathcal{V}_h} = \|\mathbf{u}_N - \mathbf{u}_N^\nu\|_2 = \frac{\sqrt{N}\delta_R}{1-N\delta_J} + \frac{N\delta_J\delta_T}{1-N\delta_J} + \mathcal{O}(\delta_T^2) + \mathcal{O}(\|\mathbf{u}_N - \mathbf{u}_N^\nu\|_2^2). \tag{48}$$

In particular, as $\|\mathbf{u}_N - \mathbf{u}_N^\nu\|_2^2 \to 0$ and $\delta_T \to 0$, $\|\mathbf{u}_N - \mathbf{u}_N^\nu\|_2 \leq \sqrt{N}\delta_R/(1-N\delta_J) + N\delta_J\delta_T/(1-N\delta_J)$.

Proof For notational convenience, we define $\delta\hat{\mathbf{u}}_N \equiv \hat{\mathbf{u}}_N - \mathbf{u}_N$ and $\delta\mathbf{u}_N^\nu \equiv \mathbf{u}_N - \mathbf{u}_N^\nu$. We appeal to the differentiability of the residual forms $\mathbf{r}_N : \mathbb{R}^N \to \mathbb{R}^N$ and $\mathbf{r}_N^\nu : \mathbb{R}^N \to \mathbb{R}^N$ and invoke the Taylor series expansion first about $\mathbf{u}_N$ and then about $\mathbf{u}_N^\nu$ to obtain

$$\begin{aligned}
&\mathbf{J}_N(\hat{\mathbf{u}}_N)^{-1}(\mathbf{r}_N(\hat{\mathbf{u}}_N) - \mathbf{r}_N^\nu(\hat{\mathbf{u}}_N)) \\
&= \mathbf{J}_N(\hat{\mathbf{u}}_N)^{-1}[\mathbf{r}_N(\mathbf{u}_N) + \mathbf{J}_N(\mathbf{u}_N)\delta\hat{\mathbf{u}}_N - \mathbf{r}_N^\nu(\mathbf{u}_N) - \mathbf{J}_N^\nu(\mathbf{u}_N)\delta\hat{\mathbf{u}}_N + \mathcal{O}(\|\delta\hat{\mathbf{u}}_N\|_2^2)] \\
&= \mathbf{J}_N(\hat{\mathbf{u}}_N)^{-1}[-\mathbf{r}_N^\nu(\mathbf{u}_N^\nu) - \mathbf{J}_N^\nu(\mathbf{u}_N^\nu)\delta\mathbf{u}_N^\nu + (\mathbf{J}_N(\mathbf{u}_N) - \mathbf{J}_N^\nu(\mathbf{u}_N))\delta\hat{\mathbf{u}}_N + \mathcal{O}(\|\delta\mathbf{u}_N^\nu\|_2^2) + \mathcal{O}(\|\delta\hat{\mathbf{u}}_N\|_2^2)].
\end{aligned} \tag{49}$$

We note that the first term in the bracket of (49) vanishes since $\mathbf{r}_N^\nu(\mathbf{u}_N^\nu) = 0$. We next note $\mathbf{u}_N^\nu - \hat{\mathbf{u}}_N = -\delta\mathbf{u}_N^\nu - \delta\hat{\mathbf{u}}_N$, appeal to the thrice differentiability of $\mathbf{r}_N^\nu : \mathbb{R}^N \to \mathbb{R}^N$ (which implies $\mathbf{J}_N^\nu : \mathbb{R}^N \to \mathbb{R}^{N\times N}$ is twice differentiable), and invoke the Taylor series expansion of the second term in the bracket of (49) about $\hat{\mathbf{u}}_N$ to obtain

$$\begin{aligned}
-\mathbf{J}_N^\nu(\mathbf{u}_N^\nu)\delta\mathbf{u}_N^\nu &= -\mathbf{J}_N^\nu(\hat{\mathbf{u}}_N)\delta\mathbf{u}_N^\nu - \mathbf{J}_N^\nu{}'(\hat{\mathbf{u}}_N; \mathbf{u}_N^\nu - \hat{\mathbf{u}}_N)\delta\mathbf{u}_N^\nu + \mathcal{O}(\|\mathbf{u}_N^\nu - \hat{\mathbf{u}}_N\|^2) \\
&= -\mathbf{J}_N^\nu(\hat{\mathbf{u}}_N)\delta\mathbf{u}_N^\nu - \mathbf{J}_N^\nu{}'(\hat{\mathbf{u}}_N; -\delta\mathbf{u}_N^\nu - \delta\hat{\mathbf{u}}_N)\delta\mathbf{u}_N^\nu + \mathcal{O}(\|\delta\mathbf{u}_N^\nu\|_2^2) + \mathcal{O}(\|\delta\hat{\mathbf{u}}_N\|_2^2) \\
&= -\mathbf{J}_N^\nu(\hat{\mathbf{u}}_N)\delta\mathbf{u}_N^\nu + \mathcal{O}(\|\delta\mathbf{u}_N^\nu\|_2^2) + \mathcal{O}(\|\delta\hat{\mathbf{u}}_N\|_2^2)
\end{aligned} \tag{50}$$

where $\mathbf{J}_N^\nu{}'(\hat{\mathbf{u}}_N; \mathbf{a})$ is the directional derivative of $\mathbf{J}_N^\nu(\cdot)$ about $\hat{\mathbf{u}}_N$ in the direction $\mathbf{a} \in \mathbb{R}^N$. We similarly appeal to the thrice differentiability of $\mathbf{r}_N : \mathbb{R}^N \to \mathbb{R}^N$ and $\mathbf{r}_N^\nu : \mathbb{R}^N \to \mathbb{R}^N$ (which implies $\mathbf{J}_N : \mathbb{R}^N \to \mathbb{R}^{N\times N}$ and $\mathbf{J}_N^\nu : \mathbb{R}^N \to \mathbb{R}^{N\times N}$ ares twice differentiable) and invoke the Taylor series expansion of the third term in the bracket of (49) about $\hat{\mathbf{u}}_N$ to obtain

$$(\mathbf{J}_N(\mathbf{u}_N) - \mathbf{J}_N^\nu(\mathbf{u}_N))\delta\hat{\mathbf{u}}_N = (\mathbf{J}_N(\hat{\mathbf{u}}_N) - \mathbf{J}_N^\nu(\hat{\mathbf{u}}_N))\delta\hat{\mathbf{u}}_N + \mathcal{O}(\|\delta\hat{\mathbf{u}}_N\|_2^2). \tag{51}$$

The substitution of (50) and (51) to (49) yields

$$\begin{aligned}
&\mathbf{J}_N(\hat{\mathbf{u}}_N)^{-1}(\mathbf{r}_N(\hat{\mathbf{u}}_N) - \mathbf{r}_N^\nu(\hat{\mathbf{u}}_N)) \\
&= -\delta\mathbf{u}_N^\nu + (I - \mathbf{J}_N(\hat{\mathbf{u}}_N)^{-1}\mathbf{J}_N^\nu(\hat{\mathbf{u}}_N))\delta\mathbf{u}_N^\nu + (I - \mathbf{J}_N(\hat{\mathbf{u}}_N)^{-1}\mathbf{J}_N^\nu(\hat{\mathbf{u}}_N))\delta\hat{\mathbf{u}}_N + \mathcal{O}(\|\delta\mathbf{u}_N^\nu\|_2^2) + \mathcal{O}(\|\delta\hat{\mathbf{u}}_N\|_2^2).
\end{aligned}$$

We then invoke the triangle inequality, note $\|\delta\hat{\mathbf{u}}_N\| \le \delta_T$ *by the condition* (43)*, and note* $\|I - \mathbf{J}_N(\hat{\mathbf{u}}_N)^{-1}\mathbf{J}_N^\nu(\hat{\mathbf{u}}_N^\nu)\|_2 \le N\|I - \mathbf{J}_N(\hat{\mathbf{u}}_N)^{-1}\mathbf{J}_N^\nu(\hat{\mathbf{u}}_N^\nu)\|_{\max} \le N\delta_J$ *by the condition* (45) *to obtain*

$$\begin{aligned}
&\|\mathbf{J}_N(\hat{\mathbf{u}}_N)^{-1}(\mathbf{r}_N(\hat{\mathbf{u}}_N) - \mathbf{r}_N^\nu(\hat{\mathbf{u}}_N))\|_2 \\
&\ge \|\delta\mathbf{u}_N^\nu\|_2 - \|I - \mathbf{J}_N(\hat{\mathbf{u}}_N)^{-1}\mathbf{J}_N^\nu(\hat{\mathbf{u}}_N)\|_2\|\delta\mathbf{u}_N^\nu\|_2 - \|I - \mathbf{J}_N(\hat{\mathbf{u}}_N)^{-1}\mathbf{J}_N^\nu(\hat{\mathbf{u}}_N)\|_2\|\delta\hat{\mathbf{u}}_N\|_2 \\
&\quad - \mathcal{O}(\|\delta\mathbf{u}_N^\nu\|_2^2) - \mathcal{O}(\|\delta\hat{\mathbf{u}}_N\|_2^2) \\
&\ge (1 - N\delta_J)\|\delta\mathbf{u}_N^\nu\|_2 - N\delta_J\delta_T - \mathcal{O}(\delta_T^2) - \mathcal{O}(\|\delta\mathbf{u}_N^\nu\|_2^2)
\end{aligned}$$

We next rearrange the expression and note $\|\mathbf{J}_N(\hat{\mathbf{u}}_N)^{-1}\mathbf{r}_N^\nu(\hat{\mathbf{u}}_N)\|_2 \le \sqrt{N}\|\mathbf{J}_N(\hat{\mathbf{u}}_N)^{-1}\mathbf{r}_N^\nu(\hat{\mathbf{u}}_N)\|_\infty \le \sqrt{N}\delta_R$ *by the condition* (47) *to obtain*

$$\begin{aligned}
\|\delta\mathbf{u}_N^\nu\|_2 &\le \frac{\|\mathbf{J}_N(\hat{\mathbf{u}}_N)^{-1}(\mathbf{r}_N(\hat{\mathbf{u}}_N) - \mathbf{r}_N^\nu(\hat{\mathbf{u}}_N))\|_2}{1 - N\delta_J} + \frac{N\delta_J}{1 - N\delta_J}\|\delta\hat{\mathbf{u}}_N\|_2 + \mathcal{O}(\delta_T^2) + \mathcal{O}(\|\delta\mathbf{u}_N^\nu\|_2^2) \\
&\le \frac{\sqrt{N}\delta_R}{1 - N\delta_J} + \frac{N\delta_J\delta_T}{1 - N\delta_J} + \mathcal{O}(\delta_T^2) + \mathcal{O}(\|\delta\mathbf{u}_N^\nu\|_2^2),
\end{aligned}$$

which is the desired bound.

We make a few remarks on Propositions 5 and 6.

Remark 7 For $\delta_T = 0$ and as $\delta_R \to 0$, the asymptotic error estimate (48) is tighter than the BRR error bound (46) by a factor of 2. Our EQP linear program $\texttt{LP}_N^\nu$ described in Section 3.3 is motivated by this asymptotic error estimate, as discussed in the next remark.

Remark 8 We relate the asymptotic error estimate Proposition 6 and in particular the three conditions — the training condition (43), the residual condition (47), and the Jacobian condition (45) — to our EQP linear program $\texttt{LP}_N^\nu$. The manifold accuracy constraints (28) is the residual condition (47) for $\hat{\mathbf{u}}_N(\mu) = \mathbf{u}_N^{\text{train}}(\mu)$ and $\delta_R = \delta/\sqrt{N}$. We next *assume* (i) the training condition $\|\mathbf{u}_N^{\text{train}}(\mu) - \mathbf{u}_N(\mu)\| \le \delta_T$ is satisfied for δ_T small. We in addition *assume* (ii) the Jacobian condition (45) is satisfied for $\delta_J \ll 1/N$. Under these two assumptions, the error is asymptotically bounded by $\|u_N - u_N^\nu\|_{\mathcal{V}_h} \le \sqrt{N}\delta_R/(1 - N\delta_J) + \delta_T \approx \delta$. Hence, the EQP linear program $\texttt{LP}_N^\nu$ directly controls the hyperreduction error *if* (i) δ_T is small and (ii) $\delta_J \ll 1/N$. We aim to satisfy condition (i) by using the bootstrapping strategy in the greedy algorithm discussed in Section 3.4, though the condition cannot be rigorously verified. We also hope the Jacobian condition (ii) is satisfied indirectly through the enforcement of the residual condition (47) by the accuracy constraints (28), though again the condition cannot be rigorously verified. We will show in Section 5 through numerical examples that in practice the EQP formulation provides control of the asymptotic error. (For a related discussion on relationships between the BRR error bound (Proposition 5) and the EQP linear program $\texttt{LP}_N^\nu$, we refer to [39].)

Remark 9 On one hand, the *stability* of the DG-RB-EQP formulation for linear hyperbolic and convection-diffusion systems is guaranteed for *any* EQP weights $\{\rho_\kappa^\nu\}_{\kappa\in\mathcal{T}_h}$ as shown in Sections 4.1 through 4.3. On the other hand, the *accuracy* of the DG-RB-EQP formulation depends on the EQP weights and in particular the tolerance used in the EQP $\texttt{LP}_N^\nu$.

5 Numerical examples

In this section we numerically assess the DG-RB-EQP formulation for three aerodynamics problems. Both the "truth" and DG-RB-EQP formulations are implemented in an in-house PDE solver, and all computations are performed on a commodity desktop.

5.1 Euler flow over a NACA 0012 airfoil

We first consider inviscid flow over a NACA 0012 airfoil modeled by the compressible Euler equations; the equations are expressed in entropy variables [7]. We consider two parameters: the angle of attack $\mu_1 \equiv \alpha \in [0°, 3°]$; and the freestream Mach number $\mu_2 \equiv M_\infty \in [0.3, 0.5]$. We note that, for $M_\infty = 0.5$ and

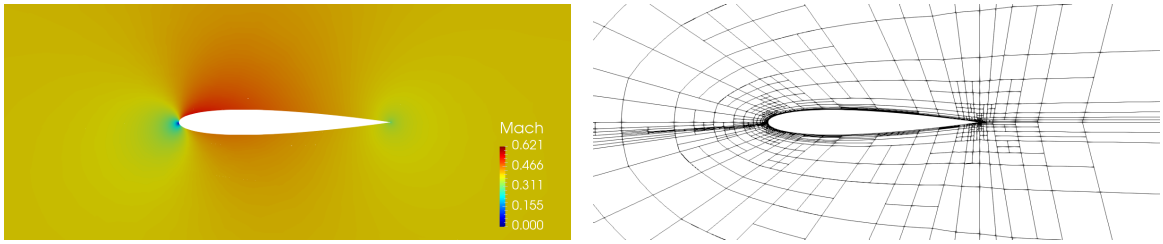

(a) solution (b) mesh

Fig. 1 The solution ($\alpha = 1.5°$ and $M_\infty = 0.4$) and the mesh for the NACA 0012 airfoil Euler problem.

$\alpha = 3°$, the local Mach number on the suction side of the airfoil exceeds 0.8 but the flow remains subsonic. Figure 1(a) shows the solution associated with the centroidal parameter value. To assess the DG-RB-EQP method for different "truth" discretizations (i.e., polynomial degree) and the training parameter set Ξ_J^{train}, we first consider a "nominal" case and then compare the result with other discretizations and training parameter set.

Nominal case. We first consider the DG-RB-EQP formulation for a "nominal" case. In this nominal case, we obtain the finite element "truth" solution using the $\mathbb{P}^2$ DG method. The mesh, which will be fixed for all parameter values, is obtained through an output-based anisotropic adaptation for the centroidal parameter value of $\alpha = 1.5°$ and $M_\infty = 0.4$ such that the error in the lift coefficient is less than 1 count (i.e., 1×10^{-4}); the initial mesh for adaptation is the mesh supplied for the NACA problem in the first AIAA high-order workshop. The "truth" space comprises 1963 $\mathbb{P}^2$ elements, and hence 47112 degrees of freedom; the mesh comprises a relatively small number of elements due to the use of a high-order method. Figure 1(b) shows the mesh in the vicinity of the airfoil. The training parameter set Ξ_J^{train} for the simultaneous greedy algorithm comprises $J = 5 \times 5$ uniformly distributed points in the parameter domain $\mathcal{D} \equiv [0°, 3°] \times [0.3 \times 0.5]$. The EQP tolerance is set to $\delta = 10^{-4}$.

Table 1(a) summarizes the behavior of the method for the case in which the test parameter set Ξ^{test} is the same as the training parameter set Ξ_J^{train}. We first observe that the number of nonzero EQP weights increases as the dimension of the reduced basis space (N) increases. We second observe that the dual norm of the "truth" residual decreases as N increases, but the convergence behavior is not monotonic; due to the use of the Galerkin projection (instead of the minimum-residual projection), we do not in general expect the residual to decrease monotonically. We third observe that the $L^2(\Omega)$ norm of the error decreases as N increases; the RB approximation and the EQP hyperreduction reduces the $L^2(\Omega)$ error by over five orders of magnitude using just $N = 11$ RB functions and 80 integration elements relative to the 47112 degrees of freedom and 1963 integration elements of the "truth" DG discretization. (We observe the rapid convergence as the flow remains subsonic; if this were a transonic flow with a parameter-dependent shock, then we would observe a much lower convergence rate as disucssed in the Introduction.) We fourth observe that the EQP hyperreduction error is controlled for $N > 7$; the maximum error for $\mu \in \Xi^{\text{test}} = \Xi_J^{\text{train}}$ in the exact-integral RB solution $u_N(\mu)$ and the RB-EQP solution $u_N^\nu(\mu)$ is bounded by 5.0×10^{-4} (including for even N), which is comparable to the target EQP tolerance of $\delta = 10^{-4}$. We finally note that PTC strategy reliably finds the DG-RB-EQP solution for all cases used in the greedy algorithm and testing in at most 13 nonlinear iterations.

Table 1(b) summarizes the behavior of the DG-RB-EQP formulation for the case in which the test parameter set $\Xi^{\text{test}} \neq \Xi_J^{\text{train}}$ comprises 30 uniformly distributed random points in the parameter domain $\mathcal{D}$. Due to the use of the relatively dense training set Ξ_J^{train} in $\mathcal{D}$, the behavior of the algorithm in this "predictive" scenario — where the test points differ from the training points — is essentially the same as "reproduction" scenario summarized in Table 1(a). As the results for $\Xi^{\text{test}} = \Xi_J^{\text{train}}$ and $\Xi^{\text{test}} \neq \Xi_J^{\text{train}}$ are similar, and the latter provides a more comprehensive assessment of the predictive setting, we set $\Xi^{\text{test}} \neq \Xi_J^{\text{train}}$ for the remainder of the section.

We now report the computational cost. For the training parameter set of size $J = 25$, the average offline training time *per greedy iteration* is ≈ 3.8 times the time for a single "truth" solve; this cost per iteration includes the cost for (i) the single "truth" solve to compute the snapshot, (ii) $J = 25$ evaluations of the dual norm of the "truth" residual for error estimation, and (iii) $J \cdot N_{\text{eqp,smooth}} = 25 \times 3$ "truth" residual evaluations to setup the EQP linear program. The average online computational reduction for the $N = 5$ and $N = 11$ cases were ≈ 170 and 110, respectively. The online computational reduction is

Table 1 Convergence behavior for the NACA 0012 airfoil Euler problem. The columns correspond to the dimension of the reduced basis space, the number of nonzero EQP weights, the dual norm of the residual, the L^2 norm of the error with respect to the FE "truth", and the L^2 norm of the error with respect to the "truth"-quadrature RB solution. For the last three columns, the reported values are the maximum values over the test set Ξ_{test}; e.g., the dual norm of the residual reported is $\sup_{\mu\in\Xi^{\text{test}}} \|r_h(u_N^\nu(\mu),\cdot;\mu)\|_{\mathcal{V}_h'}$.

(a) $p = 2$, $|\Xi_J^{\text{train}}| = 5 \times 5$, $\Xi^{\text{test}} = \Xi_J^{\text{train}}$

N	$\text{nnz}\{\rho_\kappa\}$	$\|r_h(u_N^\nu,\cdot;\mu)\|_{\mathcal{V}_h'}$	$\|u_h - u_N^\nu\|_{L^2(\Omega)}$	$\|u_N - u_N^\nu\|_{L^2(\Omega)}$
1	8	$1.68 \times 10^{+0}$	$7.48 \times 10^{+2}$	6.35×10^{-1}
3	26	2.05×10^{-1}	$9.66 \times 10^{+1}$	7.60×10^{-5}
5	41	1.06×10^{-1}	3.59×10^{-2}	1.82×10^{-3}
7	60	9.18×10^{-2}	2.72×10^{-2}	1.72×10^{-3}
9	69	1.92×10^{-1}	1.74×10^{-2}	4.93×10^{-4}
11	80	7.11×10^{-3}	1.60×10^{-3}	5.20×10^{-5}
13	93	1.00×10^{-3}	6.81×10^{-4}	1.27×10^{-4}

(b) $p = 2$, $|\Xi_J^{\text{train}}| = 5 \times 5$, $\Xi^{\text{test}} \neq \Xi_J^{\text{train}}$

N	$\text{nnz}\{\rho_\kappa\}$	$\|r_h(u_N^\nu,\cdot;\mu)\|_{\mathcal{V}_h'}$	$\|u_h - u_N^\nu\|_{L^2(\Omega)}$	$\|u_N - u_N^\nu\|_{L^2(\Omega)}$
1	8	$1.56 \times 10^{+0}$	$7.13 \times 10^{+2}$	6.05×10^{-1}
3	26	1.57×10^{-1}	$8.96 \times 10^{+1}$	6.17×10^{-5}
5	41	9.13×10^{-2}	2.91×10^{-2}	1.60×10^{-3}
7	60	7.70×10^{-2}	2.21×10^{-2}	1.62×10^{-3}
9	69	1.49×10^{-1}	1.50×10^{-2}	3.45×10^{-4}
11	80	7.14×10^{-3}	1.72×10^{-3}	4.86×10^{-5}
13	93	9.61×10^{-4}	6.78×10^{-4}	1.04×10^{-4}

(c) $p = 1$, $|\Xi_J^{\text{train}}| = 5 \times 5$, $\Xi^{\text{test}} \neq \Xi_J^{\text{train}}$

N	$\text{nnz}\{\rho_\kappa\}$	$\|r_h(u_N^\nu,\cdot;\mu)\|_{\mathcal{V}_h'}$	$\|u_h - u_N^\nu\|_{L^2(\Omega)}$	$\|u_N - u_N^\nu\|_{L^2(\Omega)}$
1	8	$1.05 \times 10^{+0}$	$7.12 \times 10^{+2}$	1.86×10^{-2}
3	22	1.01×10^{-1}	$4.96 \times 10^{+1}$	6.35×10^{-3}
5	44	9.06×10^{-2}	2.83×10^{-2}	1.28×10^{-3}
7	62	7.85×10^{-2}	2.00×10^{-2}	9.43×10^{-5}
9	83	1.36×10^{-1}	1.26×10^{-2}	1.35×10^{-4}
11	90	1.35×10^{-2}	1.33×10^{-3}	5.69×10^{-5}
13	102	2.07×10^{-3}	6.76×10^{-4}	6.02×10^{-5}

(d) $p = 2$, $|\Xi_J^{\text{train}}| = 9 \times 9$, $\Xi^{\text{test}} \neq \Xi_J^{\text{train}}$

N	$\text{nnz}\{\rho_\kappa\}$	$\|r_h(u_N^\nu,\cdot;\mu)\|_{\mathcal{V}_h'}$	$\|u_h - u_N^\nu\|_{L^2(\Omega)}$	$\|u_N - u_N^\nu\|_{L^2(\Omega)}$
1	8	$1.56 \times 10^{+0}$	$7.13 \times 10^{+2}$	6.04×10^{-1}
3	26	1.57×10^{-1}	$8.96 \times 10^{+1}$	5.69×10^{-5}
5	42	8.95×10^{-2}	2.87×10^{-2}	1.11×10^{-3}
7	67	7.39×10^{-2}	2.18×10^{-2}	9.06×10^{-5}
9	73	1.61×10^{-1}	1.52×10^{-2}	3.52×10^{-5}
11	81	7.52×10^{-3}	1.73×10^{-3}	7.99×10^{-5}
13	95	1.10×10^{-3}	7.65×10^{-4}	6.94×10^{-5}

achieved due to (i) the reduction in the number of elements involved in the residual evaluation, (ii) the elimination of large sparse linear solves, and (iii) the reduction in the number of PTC iterations; for this Euler problem with a very small element in the training edge region, the item (iii) plays a larger role in achieving the savings relative to the Navier-Stokes case considered in Section 5.3. Comparing the offline training cost and the online speedup, we may conclude that the DG-RB-EQP formulation results in an overall computational reduction in many-query scenarios that require $\gtrsim 19$ queries for $N = 5$ and that require $\gtrsim 41$ queries for $N = 11$.

Effect of the polynomial degree. We next assess how the choice of the "truth" discretization affects the performance of the DG-RB-EQP formulation. To this end, we obtain the finite element "truth" discretization using an adaptive $\mathbb{P}^1$ DG method with the lift error tolerance of 1 count; the "truth" space comprises 13511 $\mathbb{P}^1$ elements and hence 162132 degrees of freedom. Note that, for the same error level, the $\mathbb{P}^1$ mesh contains approximately seven times more elements than the $\mathbb{P}^2$ mesh due to the lower-order approximation. We now compare Tables 1(c) and 1(b); the only difference between the tables is that the former uses the $\mathbb{P}^1$ discretization and the latter uses the $\mathbb{P}^2$ discretization. We first observe that, for a given N, the number of nonzero EQP weights are comparable for both $\mathbb{P}^1$ and $\mathbb{P}^2$ discretizations,

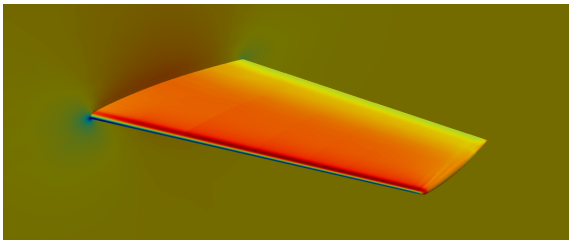

(a) solution

Fig. 2 The solution ($\alpha = 1.5°$ and $M_\infty = 0.4$) for the ONERA M6 wing Euler problem.

despite the former having seven times more "truth" elements. We second observe that the $L^2(\Omega)$ norm of the DG-RB-EQP error with respect to the "truth" solution for a given N is similar for the $\mathbb{P}^1$ and $\mathbb{P}^2$ discretizations; the result suggests that both "truth" discretizations are sufficiently accurate and "truth" solutions well approximate the true parametric manifold. We third observe that the EQP error control works equally well for the $\mathbb{P}^1$ and $\mathbb{P}^2$ discretizations. As regards the computational cost, for the given lift error level of 1 count, the $\mathbb{P}^1$ "truth" solver is approximately 10 times slower than the $\mathbb{P}^2$ "truth" solver, and hence the $\mathbb{P}^1$ discretization is not competitive for this particular problem; the longer computational time is due to (i) the larger number of elements, (ii) the slower PTC convergence due to the presence of smaller elements, and (iii) the implementation designed for higher-order discretizations. (Note that the $\mathbb{P}^1$ discretization, with a higher offline cost, achieves a larger "online speedup" than the $\mathbb{P}^2$ discretization; however, this is a misleading assessment as the "speedup" is not relative to a state-of-the-art adaptive high-order method.)

Effect of the training set. We next assess how the choice of the training set Ξ_J^{train} affects the performance of the DG-RB-EQP formulation. To this end, we consider a refined training set $\Xi_{J'=81}^{\text{train}}$ comprises 9×9 uniformly distributed points over the parameter domain $\mathcal{D}$. We now compare Tables 1(d) and 1(b); the only difference between the tables is that the former uses $\Xi_{J=25}^{\text{train}}$ and the latter uses $\Xi_{J'=81}^{\text{train}}$. We first observe that, for a given N, the number of nonzero EQP weights and the associated $L^2(\Omega)$ error are comparable for both $\Xi_{J=25}^{\text{train}}$ and $\Xi_{J'=81}^{\text{train}}$. However, we observe that the larger training set results in a tighter control of the EQP hyperreduction error. Hence, as expected, a denser training set yields better hyperreduction error control in the predictive setting. However, the cost of the "truth" residual evaluations to setup the EQP linear program is proportional to the number of training parameter points; as a result, the offline training time *per greedy iteration* is ≈ 10 times the time for a single "truth" solve for $J' = 81$, as opposed to ≈ 3.8 times for $J = 25$.

5.2 Euler flow over an ONERA M6 wing

We next consider inviscid flow over an ONERA M6 wing modeled by the compressible Euler equations. With exception of the three-dimensional geometry, the setting of the analysis is the same as the NACA 0012 case in Section 5.1. We consider two parameters: the angle of attack $\mu_1 \equiv \alpha \in [0°, 3°]$; and the freestream Mach number $\mu_2 \equiv M_\infty \in [0.3, 0.5]$. We note that the flow remains subsonic for all parameter values. We obtain the finite element "truth" solution using the $\mathbb{P}^2$ DG method. The "truth" mesh comprises 7936 elements, which translates to 396800 degrees of freedom for the $\mathbb{P}^2$ elements. Figure 2(a) shows the solution associated with the centroidal parameter value of $\alpha = 1.5°$ and $M_\infty = 0.4$. The training parameter set Ξ_J^{train} comprises $J = 5 \times 5$ uniformly distributed points in the parameter domain $\mathcal{D} \equiv [0°, 3°] \times [0.3 \times 0.5]$. The EQP tolerance is $\delta = 10^{-4}$.

Table 2 summarizes the behavior of the DG-RB-EQP formulation for the case the test parameter set Ξ^{test} comprises 30 randomly chosen points over $\mathcal{D}$; i.e., the "predictive" case in which $\Xi^{\text{test}} \neq \Xi_J^{\text{train}}$. The observed behavior for this three-dimensional flow is very similar to the observe behavior for the two-dimensional flow considered in Section 5.1. Namely, we observe that the DG-RB-EQP approximation reduces the $L^2(\Omega)$ norm of the error by over six orders of magnitude using just $N = 11$ RB functions and 89 integration elements compared to 396800 degrees of freedom and 7936 elements for the "truth" discretization. We also observe that the EQP hyperreduction error is controlled for $N \geq 7$ (including for even N) to less than 2.3×10^{-4}, with exception of the $N = 9$ case; the hyperreduction error is comparable

Table 2 Convergence behavior for the ONERA M6 wing Euler problem. The columns correspond to the dimension of the reduced basis space, the number of nonzero EQP weights, the dual norm of the residual, the L^2 norm of the error with respect to the FE "truth", and the L^2 norm of the error with respect to the "truth"-quadrature RB solution. For the last three columns, the reported values are the maximum values over the test set Ξ_{test}; e.g., the dual norm of the residual reported is $\sup_{\mu\in\Xi_{\text{test}}} \|r_h(u_N^\nu(\mu),\cdot;\mu)\|_{\mathcal{V}_h'}$.

N	$\text{nnz}\{\rho_\kappa\}$	$\|r_h(u_N^\nu,\cdot;\mu)\|_{\mathcal{V}_h'}$	$\|u_h - u_N^\nu\|_{L^2(\Omega)}$	$\|u_N - u_N^\nu\|_{L^2(\Omega)}$
1	10	$9.59 \times 10^{+0}$	$1.05 \times 10^{+2}$	1.92×10^{-3}
3	26	7.09×10^{-1}	$1.52 \times 10^{+1}$	4.49×10^{-5}
5	28	5.13×10^{-2}	8.49×10^{-3}	1.53×10^{-3}
7	50	3.21×10^{-2}	1.76×10^{-3}	1.69×10^{-4}
9	60	8.43×10^{-2}	2.83×10^{-3}	1.88×10^{-3}
11	91	1.27×10^{-2}	4.70×10^{-4}	9.57×10^{-5}
13	101	2.24×10^{-2}	2.18×10^{-4}	1.50×10^{-4}

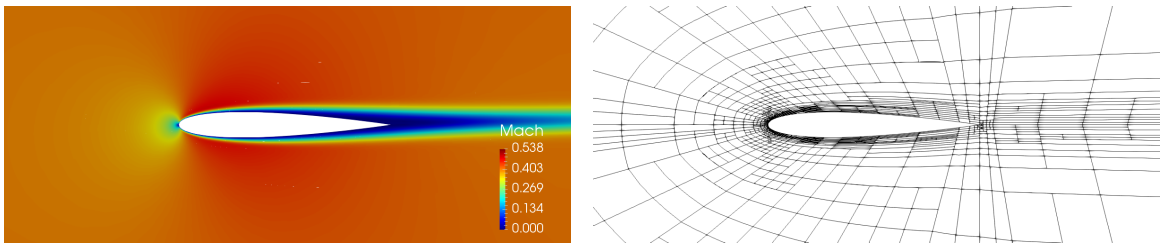

(a) solution (b) mesh

Fig. 3 The solution ($\text{Re}_c = 4000$ and $M_\infty = 0.4$) and the mesh for the NACA 0012 airfoil Navier-Stokes problem.

to the inviscid flow case considered in Section 5.1. The PTC strategy reliably finds the DG-RB-EQP solution for all training and testing cases in at most 7 nonlinear iterations.

We now report the computational cost. For the training parameter set of size $J = 25$, the offline training time per greedy iteration is approximately ≈ 4.3 times the time for a single "truth" solve; as before, the majority of the cost per iteration is associated with (i) the single "truth" solve to compute the snapshot, (ii) $J = 25$ evaluations of the dual norm of the "truth" residual for error estimation, and (iii) $J \cdot N_{\text{eqp,smooth}} = 25 \times 3$ "truth" residual evalutions to setup the EQP linear program. The average online speed up for the $N = 5$ and $N = 11$ cases were ≈ 1080 and 420, respectively. A significant speedup is achieved for this three-dimensional flow. Comparing the offline training cost and the online speedup, we may conclude that the DG-RB-EQP formulation results in an overall computational reduction in many-query scenarios that require $\gtrsim 22$ queries for $N = 5$ and that require $\gtrsim 47$ queries for $N = 11$.

5.3 Navier-Stokes flow over a NACA 0012 airfoil

We now consider viscous flow over a NACA 0012 airfoil modeled by the compressible Navier-Stokes equations; the equations are expressed in entropy variables [7]. We consider two parameters: the (chord-based) Reynolds number $\mu_1 \equiv \text{Re}_c \in [3000, 5000]$; and the freestream Mach number $\mu_2 \equiv M_\infty \in [0.3, 0.5]$. The angle of attach is fixed at $\alpha = 1°$. (As the angle of attack is fixed, the direction of the shear layer is also fixed.) We obtain the finite element "truth" solution using the $\mathbb{P}^2$ DG method. The mesh, which will be fixed for all parameter values, is obtained through an output-based anisotropic adaptation for the centroidal parameter value of $\text{Re}_c = 4000$ and $M_\infty = 0.4$ such that the error in the drag coefficient is less than 0.2 counts (i.e., 2×10^{-5}); the initial mesh for adaptation is the mesh supplied for the NACA problem in the first AIAA high-order workshop. The "truth" mesh comprises 1647 elements. Figure 3(b) shows the mesh in the vicinity of the airfoil. Figures 3(a) shows the solution associated with the centroidal parameter value. The training parameter set Ξ_J^{train} comprises $J = 5 \times 5$ uniformly distributed points in the parameter domain $\mathcal{D} \equiv [3000, 5000] \times [0.3 \times 0.5]$. The EQP tolerance is $\delta = 10^{-4}$.

Table 3 summarizes the behavior of the DG-RB-EQP formulation for the case the test parameter set Ξ^{test} comprises 30 randomly chosen points over $\mathcal{D}$; i.e., the "predictive" case in which $\Xi^{\text{test}} \neq \Xi_J^{\text{train}}$. The behavior for this viscous flow is similar to the behavior for the inviscid flow considered in Section 5.1. The DG-RB-EQP approximation reduces the $L^2(\Omega)$ norm of the error by over five orders of magnitude using just $N = 11$ RB functions and 91 integration elements compared to 39528 degrees of freedom and

Table 3 Convergence behavior for the NACA 0012 airfoil Navier-Stokes problem. The columns correspond to the dimension of the reduced basis space, the number of nonzero EQP weights, the dual norm of the residual, the L^2 norm of the error with respect to the FE "truth", and the L^2 norm of the error with respect to the "truth"-quadrature RB solution. For the last three columns, the reported values are the maximum values over the test set Ξ_{test}; e.g., the dual norm of the residual reported is $\sup_{\mu\in\Xi_{\text{test}}} \|r_h(u_N^\nu(\mu),\cdot;\mu)\|_{\mathcal{V}_h'}$.

N	$\text{nnz}\{\rho_\kappa\}$	$\|r_h(u_N^\nu,\cdot;\mu)\|_{\mathcal{V}_h'}$	$\|u_h - u_N^\nu\|_{L^2(\Omega)}$	$\|u_N - u_N^\nu\|_{L^2(\Omega)}$
1	7	$1.36 \times 10^{+0}$	$7.93 \times 10^{+2}$	8.48×10^{0}
3	17	2.70×10^{-2}	1.07×10^{-1}	5.66×10^{-4}
5	40	3.75×10^{-2}	1.42×10^{-2}	9.50×10^{-5}
7	59	1.51×10^{-2}	1.75×10^{-3}	2.03×10^{-4}
9	69	3.99×10^{-3}	6.88×10^{-4}	1.92×10^{-4}
11	89	1.95×10^{-3}	3.46×10^{-4}	1.53×10^{-4}

1647 elements for the "truth" discretization. We also observe that the EQP hyperreduction error is well controlled for $N \geq 7$; the maximum error for $\mu \in \Xi^{\text{test}} = \Xi_J^{\text{train}}$ in the exact-integral RB solution $u_N(\mu)$ and the RB-EQP solution $u_N^\nu(\mu)$ is bounded by 3.4×10^{-4} (including for even N), which is comparable to the inviscid flow case considered in Section 5.1. The PTC strategy reliably finds the DG-RB-EQP solution for all cases used in the greedy algorithm and testing in at most 10 nonlinear iterations.

We now report the computational cost. For the training parameter set of size $J = 25$, the offline training time per greedy iteration is approximately ≈ 8.4 times the time for a single "truth" solve; as before, the majority of the cost per iteration is associated with (i) the single "truth" solve to compute the snapshot, (ii) $J = 25$ evaluations of the dual norm of the "truth" residual, and (iii) $J \cdot N_{\text{eqp,smooth}} = 25 \times 3$ "truth" residual evalutions to setup the EQP linear program. The average online speed up for the $N = 5$ and $N = 11$ cases were ≈ 70 and 35, respectively. For this case, the savings is due to the reduction in the number of elements in the residual evaluation and the elimination of the elimination of large sparse linear solves; the number of required PTC iterations were similar for both the "truth" and DG-RB-EQP discretizations. Comparing the offline training cost and the online speedup, we may conclude that the DG-RB-EQP formulation results in an overall computational reduction in many-query scenarios that require $\gtrsim 42$ queries for $N = 5$ and that require $\gtrsim 92$ queries for $N = 11$.

Acknowledgements We would like to thank Prof. Anthony Patera (MIT) for many fruitful discussions and the anonymous reviewers for their helpful feedback. We acknowledge the financial support provided by the Natural Sciences and Engineering Research Council of Canada and the computational resources provided by Compute Canada/SciNet.

References

1. An, S.S., Kim, T., James, D.L.: Optimizing cubature for efficient integration of subspace deformations. ACM Trans. Graph. **27**(5), 165:1–165:10 (2008). DOI 10.1145/1409060.1409118. URL http://doi.acm.org/10.1145/1409060.1409118
2. Antonietti, P.F., Pacciarini, P., Quarteroni, A.: A discontinuous Galerkin reduced basis element method for elliptic problems. ESAIM: Mathematical Modelling and Numerical Analysis **50**(2), 337–360 (2016). DOI 10.1051/m2an/2015045
3. Arnold, D.N., Brezzi, F., Cockburn, B., Marini, L.D.: Unified analysis of discontinuous Galerkin methods for elliptical problems. SIAM J. Numer. Anal. **39**(5), 1749–1779 (2002)
4. Astrid, P., Weiland, S., Willcox, K., Backx, T.: Missing point estimation in models described by proper orthogonal decomposition. IEEE Trans Autom Control **53**(10), 2237–2251 (2008)
5. Barone, M.F., Kalashnikova, I., Segalman, D.J., Thornquist, H.K.: Stable galerkin reduced order models for linearized compressible flow. J. Comput. Phys. **228**(6), 1932–1946 (2009). DOI https://doi.org/10.1016/j.jcp.2008.11.015
6. Barrault, M., Maday, Y., Nguyen, N.C., Patera, A.T.: An "empirical interpolation" method: application to efficient reduced-basis discretization of partial differential equations. C. R. Acad. Sci. Paris, Ser. I **339**, 667—672 (2004)
7. Barth, T.J.: Numerical methods for gasdynamic systems on unstructured meshes. In: D. Kroner, M. Olhberger, C. Rohde (eds.) An Introduction to Recent Developments in Theory and Numerics for Conservation Laws, pp. 195–282. Springer-Verlag (1999)
8. Bassi, F., Rebay, S.: GMRES discontinuous Galerkin solution of the compressible Navier-Stokes equations. In: K. Cockburn, Shu (eds.) Discontinuous Galerkin Methods: Theory, Computation and Applications, pp. 197–208. Springer, Berlin (2000)
9. Brezzi, F., Rappaz, J., Raviart, P.A.: Finite dimensional approximation of nonlinear problems. part I: Branches of nonsingular solutions. Numerische Mathematik **36**, 1–25 (1980)
10. Bui-Thanh, T., Murali, D., Willcox, K.: Proper orthogonal decomposition extensions for parametric applications in compressible aerodynamics. AIAA 2003-4213, AIAA (2003)
11. Carlberg, K., Bou-Mosleh, C., Farhat, C.: Efficient non-linear model reduction via a least-squares petrov–galerkin projection and compressive tensor approximations. Int. J. Numer. Methods Eng. **86**(2), 155–181 (2011). DOI 10.1002/nme.3050. URL http://dx.doi.org/10.1002/nme.3050

12. Carlberg, K., Tuminaro, R., Boggs, P.: Preserving lagrangian structure in nonlinear model reduction with application to structural dynamics. SIAM J. Sci. Comput. **37**(2), B153–B184 (2015)
13. Cockburn, B.: Discontinuous Galerkin methods. ZAMM-Journal of Applied Mathematics and Mechanics/Zeitschrift für Angewandte Mathematik und Mechanik **83**(11), 731–754 (2003)
14. Everson, R., Sirovich, L.: Karhunen-Loève procedure for gappy data. J. Opt. Soc. Am. A **12**(8), 1657–1664 (1995)
15. Farhat, C., Avery, P., Chapman, T., Cortial, J.: Dimensional reduction of nonlinear finite element dynamic models with finite rotations and energy-based mesh sampling and weighting for computational efficiency. Int. J. Numer. Methods Eng. **98**(9), 625–662 (2014)
16. Farhat, C., Chapman, T., Avery, P.: Structure-preserving, stability, and accuracy properties of the energy-conserving sampling and weighting method for the hyper reduction of nonlinear finite element dynamic models. Int. J. Numer. Methods Eng. **102**(5), 1077–1110 (2015). DOI 10.1002/nme.4820. URL http://dx.doi.org/10.1002/nme.4820. Nme.4820
17. Grepl, M.A., Maday, Y., Nguyen, N.C., Patera, A.T.: Efficient reduced-basis treatment of nonaffine and nonlinear partial differential equations. ESAIM: M2AN **41**(3), 575–605 (2007). DOI 10.1051/m2an:2007031. URL https://doi.org/10.1051/m2an:2007031
18. Hernández, J., Caicedo, M., Ferrer, A.: Dimensional hyper-reduction of nonlinear finite element models via empirical cubature. Comput. Methods Appl. Mesh. Eng. **313**, 687–722 (2017). DOI https://doi.org/10.1016/j.cma.2016.10.022
19. Hesthaven, J.S., Rozza, G., Stamm, B.: Certified Reduced Basis Methods for Parametrized Partial Differential Equations. Springer (2016)
20. Hesthaven, J.S., Warburton, T.: Nodal discontinuous Galerkin methods. Springer New York (2008). DOI 10.1007/978-0-387-72067-8
21. Iollo, A., Lombardi, D.: Advection modes by optimal mass transfer. Physical Review E **89**(2) (2014). DOI 10.1103/physreve.89.022923
22. LeGresley, P.A., Alonso, J.J.: Investigation of non-linear projection for POD based reduced order models for aerodynamics. AIAA 2001–0926, AIAA (2001)
23. LeGresley, P.A., Alonso, J.J.: Dynamic domain decomposition and error correction for reduced order models. In: 41st Aerospace Sciences Meeting and Exhibit. American Institute of Aeronautics and Astronautics (2003). DOI 10.2514/6.2003-250
24. Nguyen, N.C., Peraire, J.: An efficient reduced-order modeling approach for non-linear parametrized partial differential equations. Int. J. Numer. Methods Eng. **76**(1), 27–55 (2008). DOI 10.1002/nme.2309. URL http://dx.doi.org/10.1002/nme.2309
25. Ohlberger, M., Rave, S.: Nonlinear reduced basis approximation of parameterized evolution equations via the method of freezing. Comptes Rendus Mathematique **351**(23-24), 901–906 (2013). DOI 10.1016/j.crma.2013.10.028
26. Ohlberger, M., Rave, S.: Reduced basis methods: Success, limitations and future challenges. In: Proceedings of the Conference Algoritmy, pp. 1–12 (2016)
27. Ohlberger, M., Schindler, F.: Error control for the localized reduced basis multiscale method with adaptive on-line enrichment. SIAM Journal on Scientific Computing **37**(6), A2865–A2895 (2015). DOI 10.1137/151003660
28. Patera, A.T., Yano, M.: An LP empirical quadrature procedure for parametrized functions. C. R. Acad. Sci. Paris, Ser. I (2017)
29. Pietro, D.A.D., Ern, A.: Mathematical aspects of discontinuous Galerkin methods. Springer Berlin Heidelberg (2012). DOI 10.1007/978-3-642-22980-0
30. Pinkus, A.: n-widths of Sobolev spaces in l^p. Constructive Approximation **1**(1), 15–62 (1985). DOI 10.1007/bf01890021
31. Quarteroni, A., Manzoni, A., Negri, F.: Reduced Basis Methods for Partial Differential Equations. Springer (2016)
32. Rivière, B.: Discontinuous Galerkin methods for solving elliptic and parabolic equations: theory and implementation. Society for Industrial and Applied Mathematics (2008). DOI 10.1137/1.9780898717440
33. Rozza, G., Huynh, D.B.P., Patera, A.T.: Reduced basis approximation and *a posteriori* error estimation for affinely parametrized elliptic coercive partial differential equations — application to transport and continuum mechanics. Arch. Comput. Methods Eng. **15**(3), 229–275 (2008)
34. Ryu, E.K., Boyd, S.P.: Extensions of gauss quadrature via linear programming. Found Comput Math **15**(4), 953–971 (2015). DOI 10.1007/s10208-014-9197-9. URL https://doi.org/10.1007/s10208-014-9197-9
35. Washabaugh, K., Amsallem, D., Zahr, M., Farhat, C.: Nonlinear model reduction for CFD problems using local reduced-order bases. AIAA 2012-2686, AIAA (2012)
36. Washabaugh, K., Zahr, M.J., Farhat, C.: On the use of discrete nonlinear reduced-order models for the prediction of steady-state flows past parametrically deformed complex geometries. AIAA 2016-1814, AIAA (2016)
37. Welper, G.: Interpolation of functions with parameter dependent jumps by transformed snapshots. SIAM Journal on Scientific Computing **39**(4), A1225–A1250 (2017). DOI 10.1137/16m1059904
38. Yano, M., Modisette, J.M., Darmofal, D.: The importance of mesh adaptation for higher-order discretizations of aerodynamic flows. AIAA 2011-3852, AIAA (2011)
39. Yano, M., Patera, A.T.: An LP empirical quadrature procedure for reduced basis treatment of parametrized nonlinear pdes. Comput. Methods Appl. Mesh. Eng. (2018)
40. Zimmermann, R., Görtz, S.: Non-linear reduced order models for steady aerodynamics. Procedia Computer Science **1**(1), 165–174 (2010). DOI https://doi.org/10.1016/j.procs.2010.04.019. ICCS 2010